



HAL
open science

13: phenomenology, present status and prospect

Mauro Mezzetto, Thomas Schwetz

► **To cite this version:**

Mauro Mezzetto, Thomas Schwetz. 13: phenomenology, present status and prospect. *Journal of Physics G: Nuclear and Particle Physics*, 2010, 37 (10), pp.103001. 10.1088/0954-3899/37/10/103001 . hal-00600764

HAL Id: hal-00600764

<https://hal.science/hal-00600764>

Submitted on 16 Jun 2011

HAL is a multi-disciplinary open access archive for the deposit and dissemination of scientific research documents, whether they are published or not. The documents may come from teaching and research institutions in France or abroad, or from public or private research centers.

L'archive ouverte pluridisciplinaire **HAL**, est destinée au dépôt et à la diffusion de documents scientifiques de niveau recherche, publiés ou non, émanant des établissements d'enseignement et de recherche français ou étrangers, des laboratoires publics ou privés.

TOPICAL REVIEW

θ_{13} : phenomenology, present status and prospect

Mauro Mezzetto

Instituto Nazionale Fisica Nucleare, Sezione di Padova,
Via Marzolo 8, 35131 Padova, Italy

E-mail: mauro.mezzetto_at_pd.infn.it

Thomas Schwetz

Max-Planck-Institute for Nuclear Physics,
PO Box 103980, 69029 Heidelberg, Germany

E-mail: schwetz_at_mpi-hd.mpg.de

Abstract. The leptonic mixing angle θ_{13} is currently a high-priority topic in the field of neutrino physics, with five experiments under way, searching for neutrino oscillations induced by this angle. We review the phenomenology of θ_{13} and discuss the information from present global oscillation data. A description of the upcoming reactor and accelerator experiments searching for a non-zero value of θ_{13} is given, and we evaluate the sensitivity reach within the next few years.

PACS numbers: 14.60.Pq

Contents

1	Introduction	3
2	General remarks on θ_{13} phenomenology	5
2.1	Notations and conventions	5
2.2	Leptonic CP violation	6
2.3	The neutrino mass hierarchy	7
2.4	θ_{13} and models for neutrino mass	7
3	Present status and possible hints for $\theta_{13} > 0$	8
3.1	The bound from the CHOOZ reactor experiment	9
3.2	Information from solar neutrinos and the KamLAND reactor experiment	10
3.3	θ_{13} and atmospheric neutrinos	12
3.4	ν_e appearance data at accelerators	14
3.5	θ_{13} in the global three-flavour fit	16
4	Description of upcoming experiments	18
4.1	Reactor experiments	18
4.1.1	Double Chooz	22
4.1.2	Daya Bay	22
4.1.3	Reno	23
4.2	Accelerator experiments	24
4.2.1	T2K	26
4.2.2	NO ν A	29
5	Phenomenology and sensitivity estimates for upcoming experiments	30
5.1	Complementarity of reactor and superbeam experiments	30
5.2	On statistical errors and systematical uncertainties	33
5.3	Sensitivity predictions for the upcoming experiments	36
5.4	On the interpretation of sensitivities for future experiments	40
6	A subsequent generation of experiments	43
7	Conclusions	46

1. Introduction

Neutrino oscillations have been firmly established in the last twelve years or so by a beautiful series of experiments with neutrinos from the sun [1–7], the Earth’s atmosphere [8, 9], nuclear reactors [10, 11], and accelerators [12, 13]. All these data can be described within a three–flavour neutrino oscillation framework, characterised by two mass-squared differences ($\Delta m_{21}^2, \Delta m_{31}^2$), three mixing angles ($\theta_{12}, \theta_{13}, \theta_{23}$), and one complex phase (δ); see section 2.1 for definitions. We know that two out of the three mixing angles are large [14],

$$\sin^2 \theta_{12} = 0.318_{-0.016}^{+0.019}, \quad \sin^2 \theta_{23} = 0.50_{-0.06}^{+0.07}. \quad (1)$$

The mass-squared differences are determined relatively accurately from the spectral data in the KamLAND [11] and MINOS [13] experiments, respectively [14],

$$\Delta m_{21}^2 = 7.59_{-0.18}^{+0.23} \times 10^{-5} \text{ eV}^2, \quad |\Delta m_{31}^2| = 2.40_{-0.11}^{+0.12} \times 10^{-3} \text{ eV}^2. \quad (2)$$

The parameters in eqs. 1 and 2 are responsible for the dominating oscillation modes observed in the experiments mentioned above.

The topic of this review is the third mixing angle, θ_{13} , whose value is not known at present, and is constrained to be small compared to the other two angles [14] (updated as of May 2010),

$$\begin{aligned} \sin^2 \theta_{13} &\leq 0.031 \quad (0.047) \\ \sin^2 2\theta_{13} &\leq 0.12 \quad (0.18) & 90\% (3\sigma) \text{ CL.} \\ \theta_{13} &\leq 10.1^\circ \quad (12.5^\circ) \end{aligned} \quad (3)$$

An important contribution to the bound on θ_{13} comes from the non-observation of disappearance of reactor electron anti-neutrinos at the scale of Δm_{31}^2 at the CHOOZ [15] and Palo Verde [16] experiments, while the final bound is obtained from the combination of global neutrino oscillation data, see e.g. [14, 17, 18]. The present information on θ_{13} is reviewed in some detail in section 3, including also a discussion of possible hints for a non-zero value [17, 19].

Maybe besides the determination of the absolute neutrino mass and the search for lepton number violation in neutrino-less double beta decay, the determination of θ_{13} is one of the next primary goals in neutrino physics. Its value is of great phenomenological as well as theoretical interest. On the phenomenological side, the possibility of CP violation in neutrino oscillations, which is a genuine three–flavour effect, depends on a non-zero value of θ_{13} . Any realistic possibility to determine the type of the neutrino mass hierarchy (i.e., the sign of Δm_{31}^2) relies on a not-too-small θ_{13} . Therefore, the results on θ_{13} from the upcoming generation of experiments will be of crucial importance for a possible subsequent high-precision neutrino oscillation facility. We briefly comment on the issues of CP violation and mass hierarchy determination in sections 2.2 and 2.3, respectively. Implications of the value of θ_{13} for neutrino mass models and flavour symmetries are briefly mentioned in section 2.4.

There are several neutrino oscillation experiments currently under construction, which are expected to start data taking soon. These are the reactor neutrino experiments

Daya Bay [20], Double Chooz [21], RENO [22] and the accelerator experiments NO ν A [23] and T2K [24]. The primary goal for all of these experiments is the discovery of the yet unknown mixing angle θ_{13} . Section 4 is devoted to a description of these five experiments, and in section 5 we discuss the related phenomenology, highlighting the different nature of the experiments ($\bar{\nu}_e$ disappearance in reactors versus $\nu_\mu \rightarrow \nu_e$ or $\bar{\nu}_\mu \rightarrow \bar{\nu}_e$ appearance in accelerators) and provide sensitivity estimates.

The results of these experiments will be essential for the planning towards a possible next generation of long-baseline neutrino experiments able to address leptonic CP violation and the neutrino mass hierarchy. This could be an upgraded super beam experiment with a huge detector, or experiments using a new source for an intense neutrino beam based on decaying particles in a storage ring, such as a neutrino factory [25] (using muons) or a beta beam [26–28] (using radioactive ions). These options are under intense study, see e.g., [29–33] and any decisions will be crucially influenced by the results of the upcoming experiments discussed in this review. We briefly discuss such future high precision facilities in section 6.

We focus in this paper on upcoming experiments which are under construction or (from current perspective) are very likely to be funded. Without going into any details, let us just mention here also other more speculative ideas towards a θ_{13} measurement. These include a high-intensity tritium source immersed into a large TPC [34, 35] or the use of Mössbauer neutrinos [36–40]. Such approaches would lead to θ_{13} oscillations at baselines of order 10 m, thanks to the low energy of neutrinos emitted in tritium decay ($Q = 18.6$ keV). Unfortunately serious practical as well as principal problems seem to make such experiments unlikely from present perspective. The observation of neutrinos from a supernova explosion might also allow some conclusions on θ_{13} , in lucky circumstances even down to values of order 10^{-5} , see for example [41–43]. Apart from the explosion of a nearby supernova this requires one or even more suitable detectors at the correct location on earth with respect to the direction of the supernova. θ_{13} in the context of leptonic unitarity triangles has been discussed in [44], implications for neutrino-less double beta decay have been considered in [45], discussions about short and long baselines electron (anti)neutrino disappearance signals have been published in [46]. Implications of θ_{13} for ultra-high energy neutrinos searched for in neutrino telescopes have been discussed e.g., in [47, 48], and θ_{13} effects for neutrinos from WIMP annihilations in the centre of the sun have been considered for example in [49, 50].

Throughout this paper we restrict ourselves to the simplest unitary three-flavour framework, and ignore the possibility of additional sterile neutrinos as well as other new physics such as non-standard neutrino interactions. Let us note that effects of sterile neutrinos are strongly constrained [51, 52] and one does not expect that they have an impact at the sensitivity level of the next generation of experiments discussed here. This might be different for a subsequent generation of high precision experiments. While model independent bounds on non-standard neutrino interactions are at the level of $10^{-2} - 10^{-1}$ [53], in typical theories beyond the Standard Model one expects them to be much smaller [54, 55], beyond the sensitivities of the experiments considered here.

2. General remarks on θ_{13} phenomenology

2.1. Notations and conventions

Three-flavour lepton mixing is described by a 3×3 unitary matrix U , the so-called PMNS mixing matrix [56, 57]. In a basis where the charged lepton mass matrix is diagonal we have

$$\nu_\alpha = \sum_{i=1}^3 U_{\alpha i} \nu_i. \quad (4)$$

Here, ν_α ($\alpha = e, \mu, \tau$) are the (left-handed) so-called ‘‘flavour fields’’ participating in charged current (CC) interactions, and ν_i ($i = 1, 2, 3$) are the neutrino mass eigenfields with definite masses m_1, m_2, m_3 , respectively. Neutrino oscillations depend on the two independent mass-squared differences $\Delta m_{21}^2, \Delta m_{31}^2$, with $\Delta m_{ij}^2 \equiv m_i^2 - m_j^2$. After absorbing unphysical phases in U by redefining charged lepton fields, one finds that U contains three complex phases. Two of these are so-called Majorana phases, which appear only in lepton number violating processes (such as for example neutrino-less double beta decay) but drop out in neutrino oscillations which depend only on the so-called Dirac phase. By convention U is parametrised by the three mixing angles $\theta_{12}, \theta_{23}, \theta_{13}$, and the Dirac phase δ in the following way:

$$U = \begin{pmatrix} 1 & 0 & 0 \\ 0 & c_{23} & s_{23} \\ 0 & -s_{23} & c_{23} \end{pmatrix} \begin{pmatrix} c_{13} & 0 & e^{-i\delta} s_{13} \\ 0 & 1 & 0 \\ -e^{i\delta} s_{13} & 0 & c_{13} \end{pmatrix} \begin{pmatrix} c_{12} & s_{12} & 0 \\ -s_{12} & c_{12} & 0 \\ 0 & 0 & 1 \end{pmatrix} D_{\text{Maj}} \quad (5)$$

$$= \begin{pmatrix} c_{12}c_{13} & s_{12}c_{13} & s_{13}e^{-i\delta} \\ -c_{23}s_{12} - s_{13}s_{23}c_{12}e^{i\delta} & c_{23}c_{12} - s_{13}s_{23}s_{12}e^{i\delta} & s_{23}c_{13} \\ s_{23}s_{12} - s_{13}c_{23}c_{12}e^{i\delta} & -s_{23}c_{12} - s_{13}c_{23}s_{12}e^{i\delta} & c_{23}c_{13} \end{pmatrix} D_{\text{Maj}}, \quad (6)$$

with the abbreviations $s_{jk} \equiv \sin \theta_{jk}$, $c_{jk} \equiv \cos \theta_{jk}$, and $D_{\text{Maj}} \equiv \text{diag}(e^{i\frac{\alpha}{2}}, e^{i\frac{\beta}{2}}, 1)$ with α and β the Majorana phases. The ranges for the mixing angles and the Dirac phase are [58] $0 \leq \theta_{jk} \leq \pi/2$ and $0 \leq \delta < 2\pi$. The evolution of the neutrino flavour state can be described by a Schrödinger-like evolution equation with the Hamiltonian

$$H_\nu = \frac{1}{2E_\nu} U \text{diag}(0, \Delta m_{21}^2, \Delta m_{31}^2) U^\dagger + \text{diag}(V, 0, 0), \quad (7)$$

where V is the effective potential in matter responsible for the MSW matter effect [59–62], with $V = \sqrt{2}G_F N_e$ where N_e is the electron density along the neutrino path. Eq. 7 holds for neutrinos, for anti-neutrinos one has to replace $U \rightarrow U^*$ and $V \rightarrow -V$. From eqs. 5, 6, 7 one can make the following observations:

- We see from eq. 6 that $|U_{e3}| = \sin \theta_{13}$. Therefore, θ_{13} controls the fraction of the electron neutrino ν_e contained in the neutrino mass eigenfield corresponding to the mass m_3 . Since $\Delta m_{21}^2 \ll |\Delta m_{31}^2|$ (see eq. 2), m_3 corresponds to the mass state separated by a larger gap from the other two mass states m_1 and m_2 . Hence, for $\theta_{13} = 0$ the electron neutrino does not mix with ν_3 and can only participate in

oscillations with Δm_{21}^2 . This means ν_e decouples from oscillations involving m_3 , i.e., oscillations with $\Delta m_{31}^2 \approx \Delta m_{32}^2$.

- Let us consider the limit $\theta_{13} \rightarrow 0$ and $\Delta m_{21}^2/|\Delta m_{31}^2| \rightarrow 0$. In this case the evolution of solar neutrinos and oscillations in the KamLAND reactor experiment are described by an effective two-flavour system of ν_e and a combination of ν_μ and ν_τ , governed by the “solar parameters” θ_{12} and Δm_{21}^2 . Oscillations of atmospheric neutrinos and in the K2K and MINOS long-baseline ν_μ disappearance experiments are described by two-flavour ν_μ - ν_τ oscillations governed by the “atmospheric parameters” θ_{23} and Δm_{31}^2 . These “atmospheric” oscillations are pure vacuum oscillations, as it is easy to see from eq. 7 that the matter potential decouples from the relevant 2×2 block of the evolution Hamiltonian in this limit.
- If $\theta_{13} > 0$ the electron neutrino participates also in oscillations with Δm_{31}^2 . Therefore, one can determine θ_{13} by looking for transitions at the “atmospheric” scale involving the electron neutrino flavour.

2.2. Leptonic CP violation

Leptogenesis [63] provides a very attractive mechanism to explain the generation of a matter–antimatter asymmetry in the early Universe. An important ingredient for this to happen is CP violation in the lepton sector. While in general there is no direct connection between the CP violation at a very high scale necessary for leptogenesis and CP violation observable in low-energy experiments, an observation of CP violation in neutrino oscillations would provide a strong hint in favour of the leptogenesis idea. Therefore, there is intense activity towards a high-precision neutrino facility able to address CP violation in oscillations [29–32].

CP violation in neutrino oscillations is a consequence of a non-trivial Dirac phase δ . From the parameterisation eq. 5 it is obvious that δ becomes unphysical if θ_{13} is zero. Leptonic CP violation will manifest itself in a difference of the vacuum oscillation probabilities for neutrinos and anti-neutrinos [64–66]

$$P_{\nu_\alpha \rightarrow \nu_\beta} - P_{\bar{\nu}_\alpha \rightarrow \bar{\nu}_\beta} = -16 J_{\alpha\beta} \sin \frac{\Delta m_{21}^2 L}{4E_\nu} \sin \frac{\Delta m_{32}^2 L}{4E_\nu} \sin \frac{\Delta m_{31}^2 L}{4E_\nu}, \quad (8)$$

where

$$J_{\alpha\beta} = \text{Im}(U_{\alpha 1} U_{\alpha 2}^* U_{\beta 1}^* U_{\beta 2}) = \pm J, \quad J = s_{12} c_{12} s_{23} c_{23} s_{13} c_{13}^2 \sin \delta \quad (9)$$

with $+(-)$ for (anti-)cyclic permutation of the indices e, μ, τ . J is the leptonic analogue to the Jarlskog-invariant in the quark sector [67], which is a unique and parameterisation independent measure for CP violation. It vanishes if any of the three mixing angles is zero. Hence, a non-zero θ_{13} is a necessary prerequisite for leptonic CP violation. A recent review on CP violation in neutrino oscillations can be found here [68].

2.3. The neutrino mass hierarchy

An important question in neutrino physics is the type of the neutrino mass hierarchy, which can be normal (NH, $\Delta m_{31}^2 > 0$) or inverted (IH, $\Delta m_{31}^2 < 0$). This question has important consequences for possible neutrino mass models, and the problem of flavour in general. Therefore, the determination of the sign of Δm_{31}^2 is among the main goals for a future long-baseline facility, see e.g. [29]. Here we comment briefly on the importance of the value of θ_{13} for this measurement.

The most promising way to distinguish these two neutrino mass spectra is to search for the matter effect in transitions due to Δm_{31}^2 . The condition for an MSW resonance is

$$\cos 2\theta_{13} = \pm \frac{2E_\nu V}{\Delta m_{31}^2}, \quad (10)$$

where $+(-)$ holds for (anti)neutrinos. For a given sign of Δm_{31}^2 , eq. 10 can be fulfilled either for neutrinos or for anti-neutrinos. Therefore, finding out whether the matter resonance due to Δm_{31}^2 occurs for neutrinos or anti-neutrinos will provide a determination of the sign of Δm_{31}^2 . As discussed above the occurrence of a matter effect in Δm_{31}^2 transitions is only possible for a non-zero θ_{13} , and hence the possibility to determine the neutrino mass hierarchy via the matter effect crucially depends on the observability of θ_{13} effects. This can be done in long-baseline experiments [69, 70] or with atmospheric neutrinos [71–74].

In principle changing the sign of Δm_{31}^2 has also implications for disappearance oscillation probabilities in vacuum, independent of the matter effect [75–77]. While this effect for muon neutrino disappearance is independent of θ_{13} , in the case of electron neutrino disappearance also these methods require a large value of θ_{13} . In practice, however, such measurements turn out to be extremely difficult, maybe unrealistic [78, 79]. For completeness we also mention the possibility to discriminate NH and IH in non-oscillation experiments, e.g. [80, 81], or from supernova neutrino observations, e.g. [41, 82–85].

2.4. θ_{13} and models for neutrino mass

On the theoretical side, the determination of θ_{13} will provide important information on the mechanism of neutrino mass generation and the flavour structure in the lepton sector. Naively one may expect that since two mixing angles are large also the third one should not be too small. Considering neutrino mass models without any flavour structure, so-called anarchical models, one does expect a value of θ_{13} close to the present bound [86]. If on the contrary experiments would indicate a very tiny value for θ_{13} one might wish to have a symmetry reason as an explanation.

The intriguing result that mixing in the lepton sector is very different from the quark sector might indicate that a special mechanism is at work to produce the peculiar values of the lepton mixing angles. For example, rather symmetric patterns for the

mixing matrix are the tri-bimaximal [87] or the bimaximal [88] mixing matrices,

$$U_{\text{tri-bimax}} = \begin{pmatrix} \sqrt{2/3} & 1/\sqrt{3} & 0 \\ -1/\sqrt{6} & 1/\sqrt{3} & 1/\sqrt{2} \\ 1/\sqrt{6} & -1/\sqrt{3} & 1/\sqrt{2} \end{pmatrix}, \quad U_{\text{bimax}} = \begin{pmatrix} 1/\sqrt{2} & 1/\sqrt{2} & 0 \\ -1/2 & 1/2 & 1/\sqrt{2} \\ 1/2 & -1/2 & 1/\sqrt{2} \end{pmatrix}. \quad (11)$$

In both cases $s_{23}^2 = 1/2$ (maximal 2-3 mixing) and $\theta_{13} = 0$. While for tri-bimaximal mixing $s_{12}^2 = 1/3$ (in perfect agreement with data, see eq. 1), for bimaximal mixing $s_{12}^2 = 1/2$, which requires significant corrections to be consistent with the experimental value.

The measured values of the mixing angles may be the result of such regular patterns. This could indicate a special symmetry among generations. There is a huge literature on flavour symmetries, which we cannot properly account for here. Popular symmetries are for example a μ - τ exchange symmetry [89,90] (note that both examples given in eq. 11 fulfil the relation $|U_{\mu i}| = |U_{\tau i}|$) or the A_4 permutation symmetry [91] (usually in context of tri-bimaximal mixing), see [92] for a recent review and references. In many cases flavour symmetries predict $\theta_{13} = 0$ in the limit where the symmetry is exact, as in the tri-bimaximal and bimaximal examples given above. However, one expects corrections to the zeroth order symmetric limit due to breaking of the symmetry, which then in general will induce a finite value for θ_{13} , see for example [93,94]. Furthermore, if the symmetry holds at some high scale, renormalisation group running will introduce deviations from the symmetric limit, see e.g. [95]. In [96] a model is discussed which allows for a quite sizeable value of θ_{13} but still preserves the tri-bimaximal predictions for θ_{12} and θ_{23} .

An alternative approach to flavour comes from Grand Unified Theories (GUTs). A priori a GUT by it self makes no statement about flavour (unless it is complemented with additional flavour symmetries). However, since quarks and leptons reside in common representations of the GUT gauge group, one obtains relations between quark and lepton masses and mixing parameters. For example, a specific model based on the SO(10) gauge group has been discussed in [97], where the predictions for θ_{13} based on GUT relations between the Yukawa matrices have been worked out explicitly. Predictions of this kind can be confronted with future measurements of θ_{13} .

In Ref. [98] a survey of many neutrino mass models has been performed, with a particular focus on the predictions for θ_{13} , see also table 1 of [99]. Here we just want to point out the importance of the θ_{13} measurement for discriminating among models. Certainly an improved determination of θ_{13} (either establishing a finite value or setting a more stringent upper bound) will provide important new information regarding the problem of flavour. Further discussion and references can be found in the review [100].

3. Present status and possible hints for $\theta_{13} > 0$

The present information on the value of θ_{13} emerges from an interplay of the global data on neutrino oscillations, as illustrated in fig. 1, see [14,18,101] for recent global

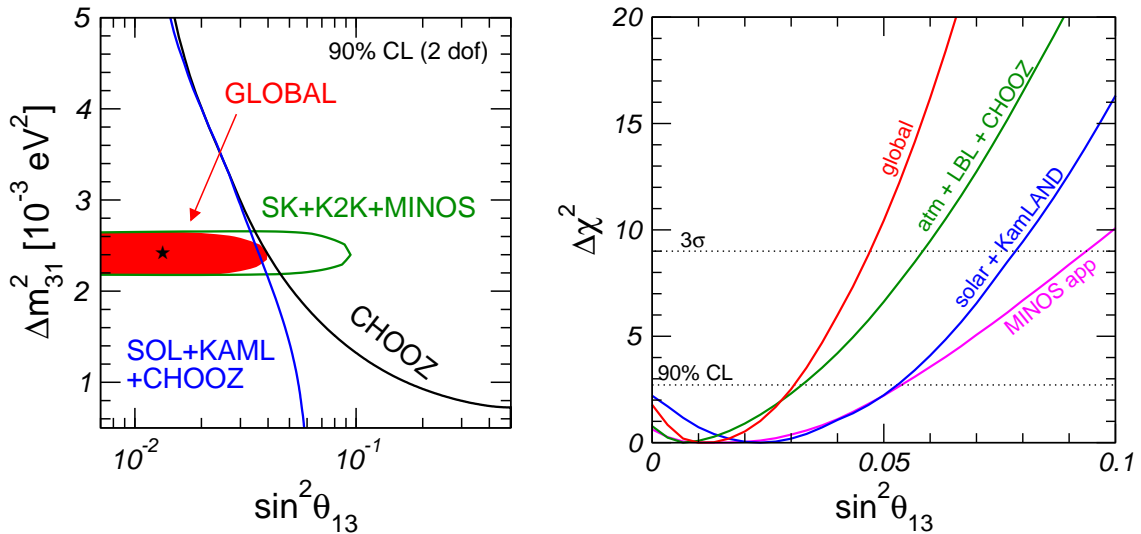


Figure 1. Constraints on $\sin^2 \theta_{13}$ from different parts of the global data [14] (updated as of May 2010).

analyses. In the following we discuss the phenomenology of the various different data sets from the CHOOZ reactor experiment (sec. 3.1), solar neutrinos and the KamLAND reactor experiment (sec. 3.2), atmospheric neutrinos (sec. 3.3), and the ν_e appearance data from the MINOS long-baseline experiment (sec. 3.4). In section 3.5 we summarise the status of θ_{13} in the global analysis.

3.1. The bound from the CHOOZ reactor experiment

An important contribution to the bound comes, of course, from the CHOOZ reactor experiment [15]. Experimental aspects and the phenomenology of θ_{13} reactor experiments will be discussed below in sections 4.1 and 5. The CHOOZ experiment observed the $\bar{\nu}_e$ flux emitted from the two cores of the Chooz nuclear power plant at a distance $L \approx 1.05$ km. The survival probability is given by

$$P_{ee} \approx 1 - \sin^2 2\theta_{13} \sin^2 \frac{\Delta m_{31}^2 L}{4E_\nu} + \mathcal{O}(\alpha^2), \quad (12)$$

with $\alpha \equiv \Delta m_{21}^2 / \Delta m_{31}^2$. Considering typical reactor neutrino energies of $E_\nu \sim 4$ MeV one finds that this experiment is sensitive to the θ_{13} induced oscillations with Δm_{31}^2 , whereas terms due to Δm_{21}^2 are suppressed by the small solar mass squared difference and can be neglected as long as $\sin^2 2\theta_{13} \gtrsim \alpha^2 \simeq 10^{-3}$. The ratio of the measured and the predicted neutrino rates in CHOOZ, averaged over the energy spectrum, has been obtained as [15]

$$R = 1.01 \pm 2.8\%(\text{stat}) \pm 2.7\%(\text{syst}). \quad (13)$$

The parameter constraint resulting from this measurement is shown in fig. 1 in the plane of $\sin^2 \theta_{13}$ and Δm_{31}^2 . A less constraining result was reported also by the Palo Verde reactor experiment [16]. A meaning full bound on θ_{13} can only be obtained by combining

the CHOOZ result with the determination of $|\Delta m_{31}^2|$ from atmospheric and long-baseline experiments. From the combined analysis of CHOOZ + atmospheric neutrino data + K2K + MINOS disappearance data one finds $\sin^2 \theta_{13} < 0.027$ at 90% CL [14].

3.2. Information from solar neutrinos and the KamLAND reactor experiment

For solar neutrinos as well as the KamLAND reactor experiment it is an excellent approximation to consider the limit $\Delta m_{31}^2 \rightarrow \infty$. Then it follows from the Hamiltonian in eq. 7 with the parametrisation for U from eq. 5, that the survival probability of electron (anti)neutrinos is given by [102–104]

$$P_{ee} \approx c_{13}^4 P_{ee}^{2\nu} + s_{13}^4, \quad (14)$$

where $P_{ee}^{2\nu}$ is a two-flavour survival probability depending on θ_{12} and Δm_{21}^2 , where the matter potential V is replaced by $c_{13}^2 V$. The s_{13}^4 term is tiny and will be neglected in the following discussion.

For the KamLAND reactor experiment the matter potential can be neglected and $P_{ee}^{2\nu}$ is just the vacuum probability:

$$P_{ee}^{\text{KamL}} \approx \cos^4 \theta_{13} \left(1 - \sin^2 2\theta_{12} \sin^2 \frac{\Delta m_{21}^2 L}{4E_\nu} \right). \quad (15)$$

This leads to an anti-correlation of $\sin^2 \theta_{13}$ and $\sin^2 \theta_{12}$ [105], see also [104,106]. For solar neutrinos one obtains simple expressions for the low and high energy part of the solar neutrino spectrum, below and above the MSW resonance in the sun at $E_\nu^{\text{res}} \approx 2$ MeV. For low energy solar neutrinos one can adopt the vacuum approximation, and averaging over the fast oscillations leads to

$$P_{ee}^{\text{solar}} \approx \cos^4 \theta_{13} \left(1 - \frac{1}{2} \sin^2 2\theta_{12} \right) \quad (\text{low energies}). \quad (16)$$

The high energy part of the spectrum undergoes the adiabatic MSW conversion inside the sun and $P_{ee}^{2\nu} \approx \sin^2 \theta_{12}$:

$$P_{ee}^{\text{solar}} \approx \cos^4 \theta_{13} \sin^2 \theta_{12} \quad (\text{high energies}). \quad (17)$$

Eq. 16 for low energy solar neutrinos shows a similar anti-correlation between $\sin^2 \theta_{13}$ and $\sin^2 \theta_{12}$ as in KamLAND, whereas for the high energy flux subject to the SNO CC/NC measurement [5,6], a positive correlation of $\sin^2 \theta_{13}$ and $\sin^2 \theta_{12}$ emerges. As discussed e.g. in [104,105], this complementarity leads to a non-trivial constraint on θ_{13} .

Here we present results from the global solar neutrino and KamLAND analysis of Ref. [14] (2010 updated arXiv version 3), where a description of the used data can be found. For technical details see also [105,107]. Fig. 2 (left) illustrates the different correlations between θ_{12} and θ_{13} from KamLAND/low energy solar and high energy solar data discussed above. The right panel shows the $\Delta\chi^2$ profiles for two different assumptions on the Standard Solar Model. The curves labeled AGSS09 and GS98 refer to low and high metallicity solar models, respectively [108], which imply slightly different predictions for the ${}^8\text{B}$ solar neutrino flux. The “default” assumption in the

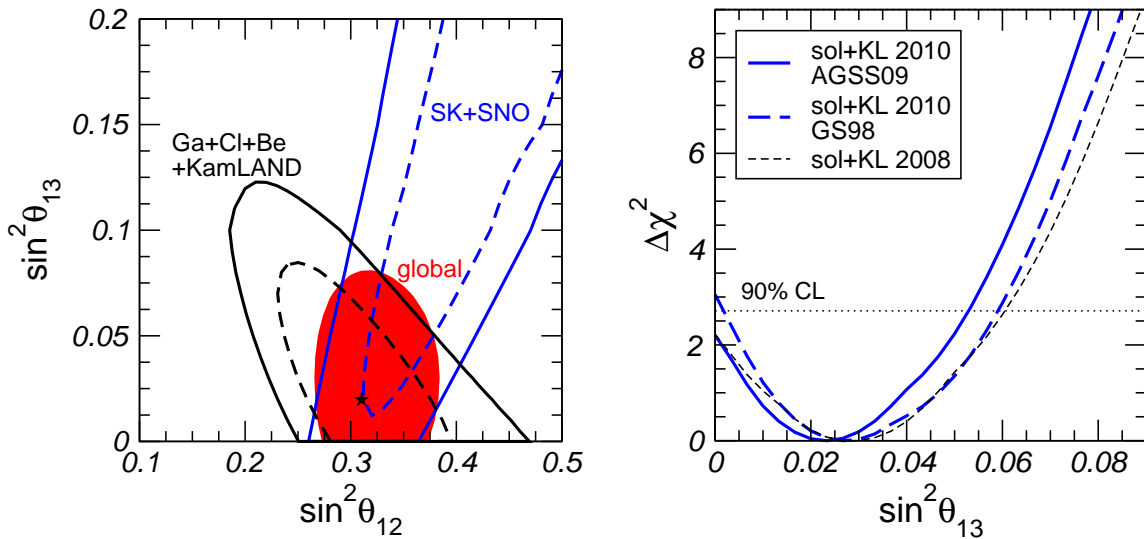


Figure 2. Left: Allowed regions in the $(\theta_{12} - \theta_{13})$ plane at 90% and 99.73% CL (2 dof). The black contours correspond to KamLAND combined with the low energy solar neutrino experiments Homestake, the Gallium experiments, and Borexino, whereas the blue contours correspond to the high energy solar neutrino experiments SuperK and SNO. The red shaded region shows the 99.73% CL region for the combined analysis. Δm_{21}^2 has been fixed at the combined best fit point. (Figure kindly produced by Mariam Tortola.) Right: $\Delta\chi^2$ as a function of $\sin^2 \theta_{13}$ for solar and KamLAND data, illustrating the impact of the most recent solar neutrino data (mainly the SNO low energy threshold analysis [6]) as well as the impact of different solar models (AGSS09 and GS98 refer to low and high metallicity solar models, respectively [108]).

global analysis of [14] is the AGSS09 low metallicity solar model. For a discussion of the impact of solar models on the fit see also [18]. Furthermore, the thin black dashed curves shows the $\Delta\chi^2$ profile for the 2008 solar neutrino analysis from [14], highlighting the impact of the most recent solar neutrino data, mainly the SNO low energy threshold analysis [6] which leads to an improved determination of the total NC event rate with the remarkable precision of 3.1% (stat) and 2.5% (syst) at 1σ .

The θ_{13} fit results [14] from global solar data and KamLAND are (best fit and 1σ errors)

$$\sin^2 \theta_{13} = 0.022_{-0.015}^{+0.018} \quad (\text{solar} + \text{KamLAND}), \quad (18)$$

and the following bound is obtained at 90% (3σ) CL:

$$\sin^2 \theta_{13} < 0.053 \quad (0.078) \quad (\text{solar} + \text{KamLAND}). \quad (19)$$

The result from eq. 18 is in excellent agreement with the value obtained by the SNO Collaboration [6], $\sin^2 \theta_{13} = 0.0200_{-0.0163}^{+0.0209}$, and it implies a slight preference for a non-zero value of θ_{13} . At $\theta_{13} = 0$ we have $\Delta\chi^2 = 2.2$ (see fig. 2), which corresponds to a hint at about 1.5σ . This hint emerges from a slight mismatch of the best fit points for θ_{12} and Δm_{21}^2 for $\theta_{13} = 0$ for solar and KamLAND data separately [17, 104, 106, 107]. This mismatch can be alleviated to some extent by a finite value of θ_{13} , see e.g. [106] for a discussion. From fig. 2 (left) we see that the high energy solar neutrino experiments

SuperK and SNO show a slight preference for a non-zero θ_{13} . Eq. 17 indicates a degeneracy among θ_{13} and θ_{12} as visible in the figure. This degeneracy is not complete due to additional information from the spectral shape as well as day-night asymmetries induced by the matter effect in the earth during night. While the χ^2 slope along the SuperK+SNO allowed region is very flat, these data pull the global best fit point somewhat towards a non-zero value. For models with higher solar metallicities like GS98, a slightly larger best fit point is obtained, $\sin^2 \theta_{13} = 0.027_{-0.015}^{+0.019}$ and $\Delta\chi^2 = 3.05$ at $\theta_{13} = 0$, while the bound on θ_{13} becomes slightly weaker, see fig. 2 (right).

3.3. θ_{13} and atmospheric neutrinos

Atmospheric neutrino data come from the SuperKamiokande experiment that recently released an updated analysis of the combined SK I+II+III data [109]. Atmospheric neutrinos provide a probe of several decades in L/E_ν thanks to the wide range in neutrino energies, from few 100 MeV to several GeV, and baselines of $L \sim 15$ km for down going neutrinos up to $L \sim 12000$ km for up-going ones. Furthermore, up-going neutrinos have large trajectories through earth matter, opening the possibility to look for matter effects. On the other hand, the atmospheric neutrino “beam” is very messy, consisting of $\nu_\mu, \bar{\nu}_\mu, \nu_e, \bar{\nu}_e$ fluxes with large uncertainties. Therefore, from the observation of muons and electrons from neutrino CC interactions one can access only certain combinations of transition and survival probabilities. Also, the neutrino direction for a given CC event is not known.

In water Čerenkov detectors such as SuperKamiokande, electron-like events provide sensitivity to three-flavour effects. One can identify three type of effects: θ_{13} -induced [71, 110–116], Δm_{21}^2 -induced [117–121], and interference effects of the previous two [119], see e.g. [122] for a discussion. Effects induced by θ_{13} are important in the multi-GeV energy range, whereas Δm_{21}^2 effects are mainly relevant for sub-GeV energies. Defining the excess of e -like events as $\epsilon_e \equiv (N_e/N_e^0 - 1)$, with N_e (N_e^0) being the number of e -like events with (without) oscillations, one has

$$\epsilon_e^{\text{multi}} \approx (r \sin^2 \theta_{23} - 1) \langle P_{31}^{2\nu} \rangle, \quad (20)$$

$$\epsilon_e^{\text{sub}} \approx (r \cos^2 \theta_{23} - 1) \langle P_{21}^{2\nu} \rangle. \quad (21)$$

Here $\langle P_{31}^{2\nu} \rangle$ ($\langle P_{21}^{2\nu} \rangle$) is an effective two-flavour probability governed by Δm_{31}^2 and θ_{13} (Δm_{21}^2 and θ_{12}), appropriately averaged and including the weighted contributions from neutrinos and anti-neutrinos, and $r(E_\nu, \Theta) \equiv F_\mu^0/F_e^0$ is the ratio of the initial unoscillated muon and electron neutrino fluxes, Θ being the zenith angle. Since for sub-GeV energies $r \approx 2$, Δm_{21}^2 effects are suppressed for $\theta_{23} \approx \pi/4$, however they provide a sensitive measure for deviations from maximal θ_{23} mixing. Indeed, small deviations from $\theta_{23} = \pi/4$ found in [122, 123] may be traced back to a slight excess of sub-GeV e -like events in the SuperKamiokande data, see, however [109], where such deviations are not found.

Here we are more interested in θ_{13} induced effects from eq. 20, relevant in the multi-GeV range, where one has $r \approx 2.6 - 4.5$. Hence one expects that these effects could show

up also for maximal θ_{23} mixing. Qualitatively, $\epsilon_e^{\text{multi}}$ vanishes for $\theta_{13} = 0$ and increases monotonically with θ_{13} . The effect is most pronounced for zenith angles corresponding to neutrino trajectories crossing the earth mantle, or earth mantle and core, where θ_{13} -effects can be resonantly enhanced due to matter effects [59, 61, 110, 111]. In the relevant zenith angle bins $\epsilon_e^{\text{multi}}$ can reach values of the order of 10% (see e.g. fig. 5 of [71]). For the normal hierarchy the resonant matter enhancement occurs for neutrinos, whereas for the inverted hierarchy it occurs for anti-neutrinos. Since the event numbers in water Čerenkov detectors are dominated by neutrinos because of larger cross sections, $\epsilon_e^{\text{multi}}$ is larger by a factor of 1.5 – 2 for the normal hierarchy than for the inverted one.

In addition to Δm_{21}^2 -effects of eq. 21 and θ_{13} -effects of eq. 20 also an interference term between the two contributions is present [119]. It is proportional to $(r \sin \theta_{13} \sin 2\theta_{23})$, it vanishes in the limit $\Delta m_{21}^2 = 0$, and it depends on the CP-phase δ . Because of the different dependence on the flux ratio r the interference term may become important in cases where the effects governed by eqs. 21 and 20 are suppressed [122].

Such three-flavour effects in atmospheric neutrinos can be used to determine the neutrino mass hierarchy or the octant of θ_{23} (if different from $\pi/4$), in huge future atmospheric neutrino detectors (e.g., water Čerenkov or magnetised iron), possibly in combination with a future long-baseline experiment, see for example [72–74, 124–126]. In the following we discuss possible implications of present data from SuperKamiokande (SK) on θ_{13} .

In Ref. [122] a preference for a non-zero θ_{13} value from SK-I data was noted (see also [127]). Refs. [17, 101, 122] find from atmospheric + CHOOZ + long-baseline disappearance data a 0.9σ hint for a non-zero value: $\sin^2 \theta_{13} = 0.012 \pm 0.013$. In the atmospheric neutrino analysis in [14] which is based on [105] Δm_{21}^2 effects are neglected, and combined with CHOOZ data the best fit occurs for $\theta_{13} = 0$ (c.f. fig. 3, right). This is in agreement with a similar analysis by the SuperKamiokande collaboration [109, 128]. Also, in the atmospheric neutrino analysis from Ref. [123] (which does include Δm_{21}^2 effects, as Refs. [17, 122]) the preference for a non-zero θ_{13} is much weaker than the one from [122], with a $\Delta\chi^2 \lesssim 0.2$.

A discussion and comparison of the results of different groups can be found in [129]. The possible origin of the hint from atmospheric data has been investigated in some detail in [18, 130]. Ref. [130] concludes that the statistical relevance of the hint for non-zero θ_{13} from atmospheric data depends strongly on the details of the event rate calculations and of the χ^2 analysis (such as e.g., the specific way of how systematic uncertainties are treated). Furthermore, the reason for the hint seems to be a small excess of multi-GeV e -like events in SK-I data (used in [17, 122]), which however disappears after the inclusion of SK-II data. Ref. [18] comes to a similar conclusion from the combined SK-I+II+III data.

Let us stress, however, that all analyses agree within $\Delta\chi^2 \approx 1$ and therefore there is no significant disagreement. Certainly these are very subtle effects sensitive to the fine details of the data analysis which can be addressed optimally only within the experimental collaboration. The recent three-flavour analysis by

SuperKamiokande [109] did not find any hint for a non-zero θ_{13} . The θ_{13} analysis of [109] has been performed adopting the approximation $\Delta m_{21}^2 = 0$, and therefore, a direct comparison with the results of the phenomenological groups [17, 18, 122, 123, 130] is still not possible.

3.4. ν_e appearance data at accelerators

The first result on ν_e appearance at a long baseline experiment has been published by the K2K collaboration [131]: $\sin^2 2\theta_{13} \geq 0.3$ (90% CL) in a two-flavour approximation analysis. Now also the MINOS experiment provides a first glance at a $\nu_\mu \rightarrow \nu_e$ appearance search for θ_{13} [19], which is actually the main objective for the upcoming T2K and NO ν A experiments, see section 4.

In Ref. [19] a search for $\nu_\mu \rightarrow \nu_e$ transitions by the MINOS experiment has been presented, based on a 3.14×10^{20} protons-on-target (pot) exposure in the Fermilab NuMI beam (out of the 7×10^{20} pot accumulated so far). 35 events have been observed in the far detector with a background of $27 \pm 5(\text{stat}) \pm 2(\text{syst})$ events predicted by the measurements in the near detector. This corresponds to an excess of about 1.5σ which can be interpreted as a weak hint for ν_e appearance due to a non-zero θ_{13} . ‡

In the MINOS detector, being optimised for muons, it is rather difficult to identify ν_e CC events since they lead to an electromagnetic shower not very different from a π^0 signal. Neutral current (NC) and misidentified ν_μ CC events often have a similar signature, and hence lead to a background for the ν_e appearance search. Indeed, in Ref. [132] an analysis of “NC events” has been performed, where “NC events” in fact include also ν_e CC events due to the similar event topology. Therefore, a possible $\nu_\mu \rightarrow \nu_e$ oscillation signal would contribute to the “NC event” sample of [132] and these data can be used to constraint θ_{13} .

We have performed a fit to the MINOS ν_e appearance and NC data by using the GLoBES simulation software [133, 134]. The predicted ν_e appearance spectrum has been calibrated by using the information given in [135]. In the fit we include a 7.3% uncertainty on the background normalisation (Tab. I of [19]). For the NC analysis we have performed a fit to the observed spectrum by summing the NC events induced from the total neutrino flux with the ν_e CC appearance signal due to oscillations. We include a 4% error on the predicted NC spectrum and a 3% error on the ν_μ CC induced background (Tab. II of [132]). A full three-flavour fit is performed taking into account a 5% uncertainty on the matter density along the neutrino path.

The $\nu_e \rightarrow \nu_\mu$ oscillation probability depends in a non-trivial way on all 6 oscillation parameters, in particular on the unknown value of the CP-phase δ as well as on the sign of Δm_{31}^2 (neutrino mass hierarchy). The dependence has to be taken into account when extracting information on θ_{13} . This will be discussed in more detail in section 5

‡ We note however that the signal excess depends very much on the choice of the position of the cut on the neural network variable that separates signal from backgrounds (fig. 2 of reference [19]). Also for this reason the publication of the ν_e appearance result with the full statistics is quite important.

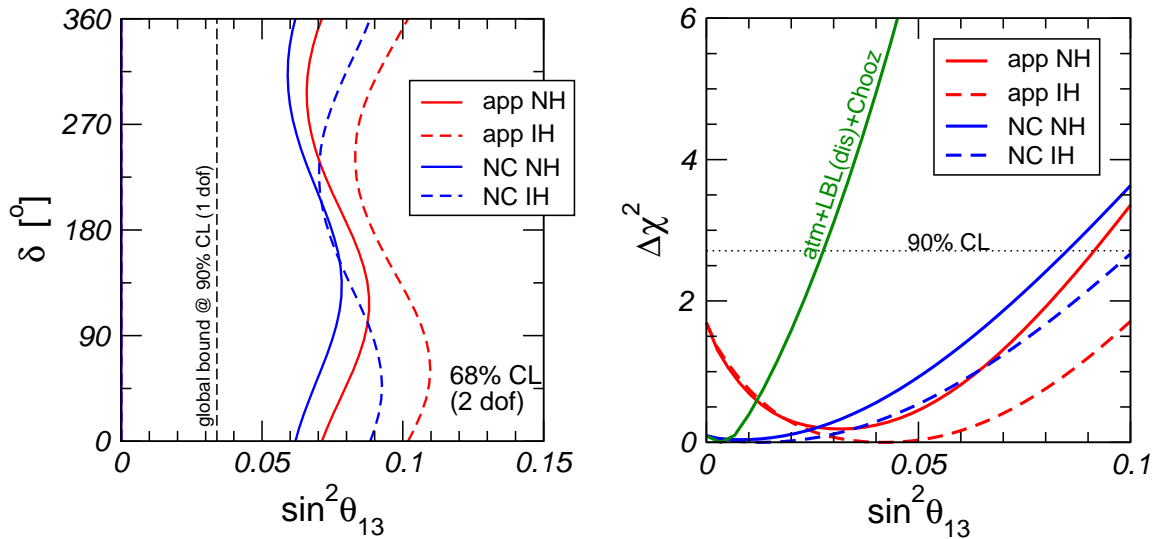


Figure 3. Left: Allowed regions in the $(\sin^2 \theta_{13} - \delta)$ plane at 68% CL (2 dof) for MINOS ν_e appearance and NC data. Regions are shown separately for normal (NH) and inverted (IH) neutrino mass hierarchy. For comparison we show also the bound from global data at 90% CL (1 dof). Right: $\Delta\chi^2$ projection as a function of $\sin^2 \theta_{13}$ for MINOS ν_e appearance and NC data, assuming NH (solid) and IH (dashed), both with respect to the common minimum, which occurs for IH. The green solid curve corresponds to the bound from CHOOZ + atmospheric + K2K + MINOS (disappearance) data.

in the context of the upcoming long-baseline accelerator experiments. Fig. 3 shows the fit results for MINOS ν_e appearance and NC data, illustrating the importance of the parameter correlations. The left panel shows the allowed regions in the $(\sin^2 \theta_{13} - \delta)$ plane, for both neutrino mass hierarchies separately. We observe the typical S-shaped regions coming from the trigonometric dependence on the phase δ . In the right panel the χ^2 is marginalised with respect to all parameters except for θ_{13} and $\text{sgn}(\Delta m_{31}^2)$, where for the solar and atmospheric parameters we imposed Gaussian errors taken from eqs. 1, 2, without including any other information on θ_{13} except from MINOS itself.

First, we note that the best fit point is always obtained for the inverted hierarchy ($\Delta m_{31}^2 < 0$), and in that case in general the constraint on $\sin^2 \theta_{13}$ is weaker, since for IH the matter effect tends to suppress the ν_e appearance probability. In fig. 3 (right) the $\Delta\chi^2$ for normal hierarchy ($\Delta m_{31}^2 > 0$) is given with respect to the best fit for IH. In the global analysis we also marginalise over the two hierarchies, and hence, the actual information from MINOS comes from the IH.

Second, we see from the figure that MINOS ν_e appearance data shows a slight preference for a non-zero value of θ_{13} , with a best fit point of $\sin^2 \theta_{13} = 0.032(0.043)$ for NH (IH) with $\Delta\chi^2 = 1.8$ at $\sin^2 \theta_{13} = 0$ (about 1.3σ). In contrast, no indication for a non-zero θ_{13} comes from the NC data. Furthermore, one observes that NC gives a slightly more constraining upper bound on $\sin^2 \theta_{13}$ than ν_e appearance, while both are significantly weaker than the bound from ν_μ disappearance data + CHOOZ. Let

us mention that the result for the NC analysis strongly depends on the value assumed for the systematic uncertainty, whereas the ν_e appearance result is more robust with respect to systematics, being dominated by statistics.

MINOS ν_e and NC data are not independent, and adding the corresponding χ^2 's would imply a double counting of the same data. Therefore, only ν_e appearance data without the information from NC data is used in the global analysis of [14]. It is found, however, that adding both MINOS data sets (ignoring the double counting problem) leads to practically the same result in the global fit, both for the “hint” for $\theta_{13} > 0$ as well as the global bound, the latter being dominated by other data sets.

The OPERA experiment [136] at the CERN to Gran Sasso (CNGS) beam has an excellent electron neutrino selection efficiency, but the beam setup is optimised for ν_μ - ν_τ transition searches, being not very competitive for electron neutrino appearance searches. OPERA sensitivities to θ_{13} have been firstly computed in [137] and then in [138] where a sensitivity of $\sin^2 2\theta_{13} \geq 0.14$ (90% C.L., for $\Delta m_{31}^2 = 10^{-3} \text{ eV}^2$) has been estimated in a 5 years neutrino run at the nominal CNGS intensity of $4.5 \cdot 10^{19}$ pot/year (expected to happen after 2013). Possible upgrades of CNGS have been studied in [139, 140] where an off-axis liquid argon detector would detect neutrinos at the first oscillation maximum. For a discussion of these experimental possibilities see [141] and also section 6.

Note added: After the completion of this review the ν_e appearance data from MINOS corresponding to 7×10^{20} pot has been made public [142]. 54 events are observed with an expected background of $49.1 \pm 7.0 \pm 2.7$. The 1.5σ excess found initially in [19] has reduced now to about 0.7σ and data are therefore in perfect agreement with background expectations for no ν_e appearance. The results and figures in this section correspond to the initial 3.14×10^{20} pot, while final results on θ_{13} in the global analysis from [14] have been updated with the 7×10^{20} pot data.

3.5. θ_{13} in the global three-flavour fit

Let us now summarise the present situation obtained in the global fit of all relevant oscillation data, as illustrated in fig. 1. In the updated analysis§ of [14] the following bounds at 90% (3σ) CL are obtained (c.f. fig. 1, right):

$$\sin^2 \theta_{13} \leq \begin{cases} 0.053 (0.078) & \text{solar+KamLAND} \\ 0.033 (0.058) & \text{CHOOZ+atm+K2K+MINOS} \\ 0.031 (0.047) & \text{global data} \end{cases} \quad (22)$$

§ The results presented here are based on the arXiv version 3 of [14], updated with the 7×10^{20} pot MINOS ν_e appearance results from [142].

reference	best-fit and 1σ errors	significance
Fogli et al. [101]	$\sin^2 \theta_{13} = 0.02 \pm 0.01$	2σ
Gonzalez-Garcia et al. [18] (GS98)	$\sin^2 \theta_{13} = 0.0095^{+0.013}_{-0.007}$	1.3σ
Gonzalez-Garcia et al. [18] (AGSS09)	$\sin^2 \theta_{13} = 0.008^{+0.012}_{-0.007}$	1.1σ
Schwetz et al. [14] (GS98)	$\sin^2 \theta_{13} = 0.013^{+0.013}_{-0.010}$	1.5σ
Schwetz et al. [14] (AGSS09)	$\sin^2 \theta_{13} = 0.010^{+0.013}_{-0.008}$	1.3σ

Table 1. Comparison of the best-fit values for $\sin^2 \theta_{13}$ and the significance of the hint for $\theta_{13} > 0$ from different global fits to neutrino oscillation data. The numbers from [18] and [14] include 7×10^{20} pot ν_e appearance data from MINOS, whereas [101] is based on 3.14×10^{20} pot. AGSS09 and GS98 refer to low and high metallicity solar models, respectively [108].

The “hint” for $\theta_{13} > 0$ coming from the different data sets can be quantified by considering the $\Delta\chi^2$ for $\theta_{13} = 0$:

$$\Delta\chi^2(\theta_{13} = 0) = \begin{cases} 2.2 & (1.5\sigma) & \text{solar+KamLAND} \\ 0.8 & (0.9\sigma) & \text{CHOOZ+atm+K2K+MINOS} \\ 0.6 & (0.7\sigma) & \text{MINOS } \nu_e \text{ appearance} \\ 1.8 & (1.3\sigma) & \text{global data} \end{cases} \quad (23)$$

In table 1 we compare the best-fit values for $\sin^2 \theta_{13}$ and the significance of the hint for $\theta_{13} > 0$ from the global fits to neutrino oscillation data from three different groups. All groups find a non-zero best-fit point in the range $\sin^2 \theta_{13} = 0.01 - 0.02$. Depending on the analysis as well as variations in assumptions about the solar metallicity used as input for the solar neutrino flux prediction a “significance” for a non-zero θ_{13} between 1.1σ and 2σ is found. Part of the differences can be attributed to differences in the atmospheric neutrino analyses, as discussed in section 3.3. However, it is the opinion of the authors that within the accuracy which one can attribute to global analyses of this kind the results are in agreement. While it is premature to draw strong conclusions from these results, upcoming experiments will answer very soon the question whether θ_{13} is indeed in the range indicated by present global analyses. This will be the topic of most of the remaining part of this review.

Let us also mention that there are some limitations of the statistical method applied to obtain these results. All three groups quoted in table 1 use a $\Delta\chi^2$ method to evaluate allowed regions as well as upper bounds on θ_{13} assuming standard χ^2 -distributions. For example, the 90% CL bound is obtained by the requirement $\Delta\chi^2 = 2.71$. The confidence levels obtained by this method are only approximate close to the physical boundary of a parameter, such as $\sin^2 \theta_{13} \geq 0$ in our case of interest. The confidence interval from such a $\Delta\chi^2$ method should be interpreted as a two-sided confidence interval, which lacks a well defined meaning close to the boundary. Therefore, the results on θ_{13} quoted in this section should be taken with some grain of salt, and in particular the numbers given for various confidence levels (for the significance of a hint for a non-zero θ_{13} as well as upper bounds on θ_{13}) have to be considered only as approximate, and should always be

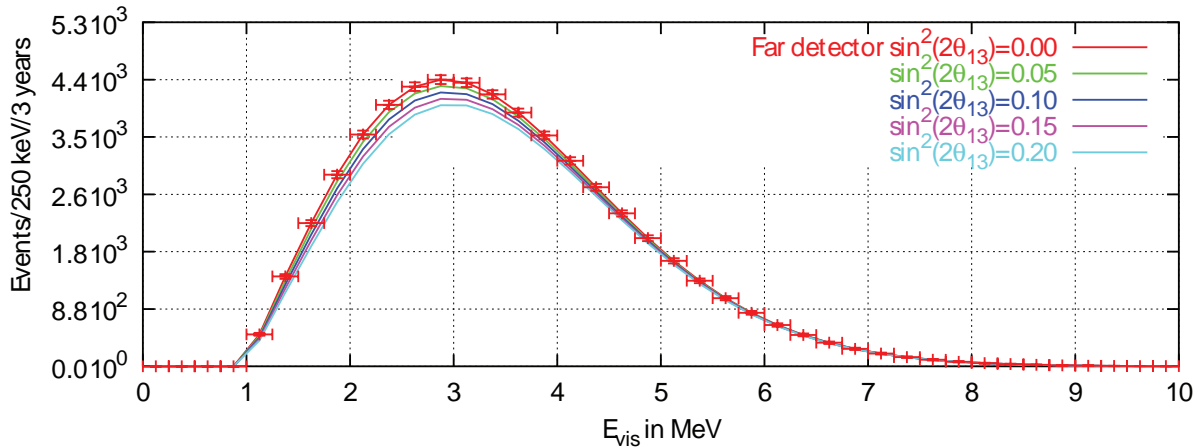


Figure 4. Neutrino induced positron spectrum for various values of $\sin^2 2\theta_{13}$ simulated for the Double Chooz far detector [143].

understood in terms of the $\Delta\chi^2$ values. To convert the $\Delta\chi^2$ values into a well defined probability would require more elaborate statistical methods than used so far in the literature.

4. Description of upcoming experiments

We move now to the discussion of the upcoming generation of experiments searching for θ_{13} , reviewing some general principles of reactor experiments (sec. 4.1) and accelerator neutrino beam experiments (sec. 4.2). In both cases we present the representatives of these classes of experiments: Daya Bay [20], Double Chooz [21], RENO [22] for the reactor experiments, and NO ν A [23] and T2K [24] for the beams.

4.1. Reactor experiments

Reactor experiments see a large signal of $\bar{\nu}_e$ events, and search for a small deviation from the non-oscillation prediction due to θ_{13} -induced $\bar{\nu}_e$ disappearance, see fig. 4. This is a precision experiment, whose success relies on statistical as well as systematical errors below the percent level.

The detection of nuclear reactor anti-neutrinos is a rather well known topic, since neutrinos themselves have been discovered at a nuclear reactor in 1956 [144]. Modern experiments are all inspired by the CHOOZ detector [145], and this technique is nicely described in [146]. Here we will very briefly summarise the basic principles.

The signal of a reactor anti-neutrino is provided by the reaction

$$\bar{\nu}_e + p \rightarrow e^+ + n, \quad (24)$$

a process with a threshold energy of 1.8 MeV where the positron provides a prompt signal (boosted by the two 511 keV annihilation gamma rays) and the neutron a delayed signal (in liquid scintillator this delay is about 170 μ s). The coincidence of the two signals

is powerful enough to make it possible to run the experiment with a tolerable level of backgrounds.

Liquid scintillator can be loaded with 0.1% natural gadolinium, an element with high thermal neutron capture cross-section. In this way the neutron capture time is reduced from $\sim 170 \mu\text{s}$ to $\sim 27 \mu\text{s}$, allowing for the reduction of the uncorrelated background. Furthermore, Gd de-excitation after capture releases an 8 MeV γ cascade (it would be ~ 2 MeV in pure liquid scintillator), producing an integrated signal well above the natural radioactivity.

The CHOOZ experiment concluded its data taking with a 2.8% statistical and a 2.7% systematical error (c.f. eq. 13). The goals of a follow-up experiment are to improve CHOOZ sensitivity by a factor 5 at least. This roughly reflects on a factor five improvement both in statistics and in systematics.

Let's start on the easy part, the statistics. The CHOOZ detector was a 5 ton detector exposed to two reactors of 8.6 MW thermal power at a distance of 1.05 km. The experiment integrated a total run of 8761.7 h, only 1543.1 of which with the two reactors on and 3245.8 h with one of the two reactors on. To gain a factor 25 in the number of neutrinos a detector twice as big running 3 years with an improved efficiency is needed. The main limiting factor in this direction is the stability of a gadolinium doped liquid scintillation detector. Important progress has been made in this field in recent years [147] such that a running time of 5 or more years seems feasible.

More generally the number of events can be estimated by

$$N \simeq 23\,000 \left(\frac{L}{\text{km}}\right)^{-2} \left(\frac{T}{\text{yr}}\right) \left(\frac{P_{\text{th}}}{\text{GW}}\right) \left(\frac{M}{100\text{ t}}\right), \quad (25)$$

where L is the baseline, T is the running time of the experiment, P_{th} is the thermal power of the nuclear power plant, M is the fiducial detector mass, and we have assumed 100% efficiency.

More difficult is the reduction of systematics. This task is particularly challenging because CHOOZ had the very rare opportunity of directly measuring the backgrounds with the nuclear reactors off. For a complete discussion and comparison of systematic errors at reactor experiments see [148].

The first important action is to introduce a close detector as similar as possible to the far detector [149–152], in order to measure the neutrino interaction rate before oscillations. In this way uncertainties on the neutrino rates (around 2%) almost cancel out. This approach has some intrinsic limitations. The neutrino rates can't be the same in the two detectors (even in absence of oscillation) because of the different coverage and of the different distance from the source. The calibration and live-time of the detectors must be kept as similar as possible. In a configuration where more than one reactors are present, the close detector doesn't measure the identical flux of the far one. This is because the neutrino flux of a reactor varies in time according to the core composition which differs from reactor to reactor following their fuel refurbishment.

The backgrounds of reactor neutrino experiments are of two types: uncorrelated signals from cosmic rays and natural radioactivity and correlated signals from neutrons

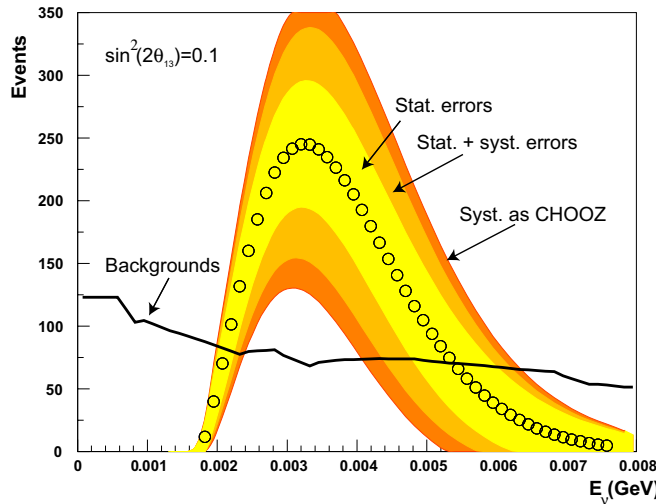


Figure 5. Number of disappeared events in Double Chooz for $\sin^2 2\theta_{13} = 0.1$, i.e., the difference between no-oscillation and oscillation spectra in the far detector, compare fig. 4. Also shown are statistic and expected systematic errors, together with systematic errors as big as the former Chooz experiment. The signal is compared to the expected background rate. Based on data from [21].

generated by cosmic muons. Uncorrelated signals can be separately measured and normalised. Their random coincidences can generate background events that can be kept at a negligible level with a careful choice of low activity materials and design of the detector.

More problematic are neutrons induced by cosmic muons. A cosmic muon not crossing the detector can induce spallation or be captured on the materials outside the detector. These can produce neutrons that escape the vetoes and produce correlated signals inside the detector that can mimic the anti-neutrino signals. Among the cosmogenically produced isotopes there are some long lived, as ^8He and ^9Li , with decay times of 119 ms and 174 ms respectively [153], that make hardware active vetoes impractical. As an example, the close detector of RENO is expected to have a 25% dead time for a 0.5 ms veto after any detected muon in the outer veto. This is the main reason that forces detectors to run at shallow depth, complicating very much the choice of the possible sites.

Fig. 5 illustrates the size of the disappearance signal in Double Chooz, compared to statistical and systematic errors as well as the expected background. Even if clearly inspired by the CHOOZ design, next generation reactor neutrino detectors have introduced improvements in the design in order to reduce the primary sources of systematics: knowledge of the fiducial volume and backgrounds.

In the following, as an example, we will describe the detector of the Double Chooz experiment, shown in fig. 6. The inner detector is made of 10.3 m^3 (8.3 metric tons, with a diameter of 2.3 m) of Gd-loaded (0.1%) liquid scintillator in an acrylic vessel. It is immersed in a gamma catcher of 22 m^3 (3.4 m of diameter) of undoped scintillator, aimed to detect the gammas emitted in both the neutron-capture process and positron

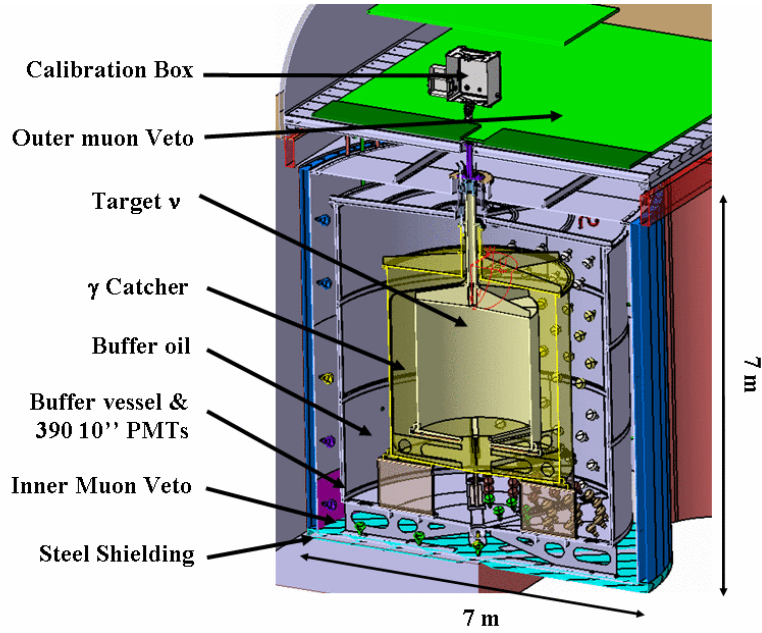


Figure 6. Sketch of the Double Chooz detector design [21].

Setup	P_{Th} [GW]	L [m]	m_{Det} [t]	Events/year	Backgrounds/day
Daya Bay [20]	17.4	1700	80	$10 \cdot 10^4$	0.4
Double Chooz [21]	8.6	1050	8.3	$1.5 \cdot 10^4$	3.6
RENO [22]	16.4	1400	15.4	$3 \cdot 10^4$	2.6

Table 2. Summary of experimental key parameters of upcoming reactor neutrino experiments. We give the thermal reactor power, the approximate distance between reactors and far detector, and detector mass, neutrino events per year, and background events per day, all for the far detector. RENO backgrounds are the sum of correlated backgrounds as computed in [22] and uncorrelated backgrounds as estimated in [148].

annihilation in the target. In this way gammas emitted from signal neutrino events in the outer volume of the target are detected, providing a well-defined target volume. A third shield of non-scintillating paraffin oil, 5.5 m diameter, separates the active target and the gamma catcher from the photo-multipliers, greatly reducing the intrinsic radioactivity of the 390 10-inch photo-multipliers, the most radioactive component of the detector (this third shield was not installed inside the CHOOZ detector). The outer detector volume is steel walled, 6.6 m diameter, filled with scintillator and lined with 70 8-inch photo-multipliers, equipping the Inner Veto, having the purpose of detecting and tracking muons and fast neutrons. An Outer Veto is placed on top of the detector, made of strips of plastic scintillator and wavelength-shifting fibres. Its task is to tag muons interacting around the detector producing cosmogenic isotopes, some of which produce correlated backgrounds in the inner detector, the most dangerous source of backgrounds for the experiment.

Below we describe briefly the three next generation reactor experiments.

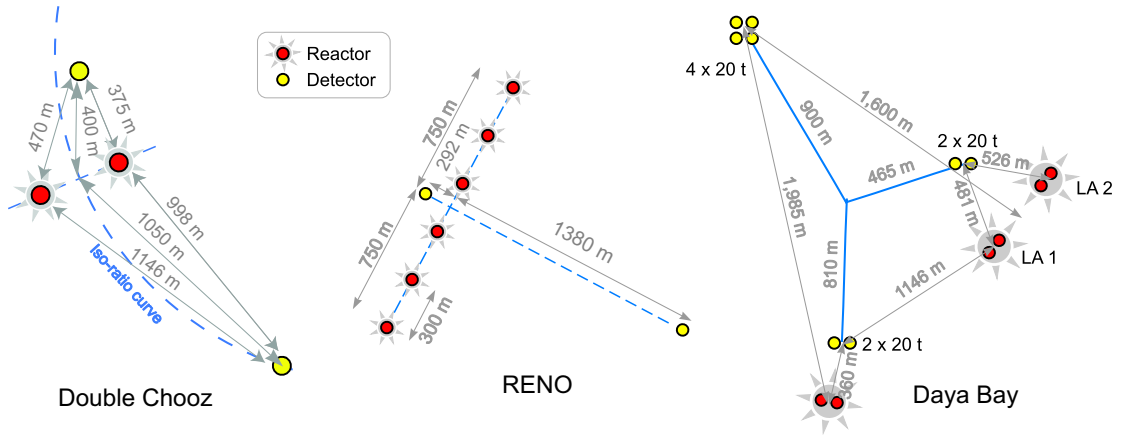


Figure 7. Configuration of the experimental layout of Double Chooz, RENO, and Daya Bay. The dashed curve in the Double Chooz configuration is the far flux iso-ratio curve. Updated from [148].

Table 2 summarises a few key parameters and fig. 7 illustrates the reactor/detector configurations.

4.1.1. Double Chooz The Double Chooz experiment [21] is being installed near the Chooz two-core (4.27+4.27 GW) nuclear power plant. The far detector, described in the previous section, is at 1.05 km from the two reactor cores, in the same site as the original CHOOZ experiment, at a depth of about 300 m.w.e. (meters of water equivalent). The close detector is designed to be identical to the far detector, it is placed 400 m from the two reactors, at a depth of 115 m.w.e., see fig. 7. Let us mention that for $\Delta m_{31}^2 \simeq 2.5 \times 10^{-3} \text{ eV}^2$ the far detector distance of 1 km is somewhat too short, shifting the oscillation signal to the lower part of the spectrum, whereas the near detector distance of 400 m is somewhat too far, with some effect of oscillations already present, see e.g. [152] for far and near detector baseline optimisation studies.

The number of neutrinos detected in the far detector assuming 3 years running time will be $\simeq 45000$ compared to 2700 in the Chooz experiment, reducing the statistical error from 2.8% to 0.47%. The goal about systematic errors is to reach a level of 0.6%. Without the near detector the systematic error would be about 2.5%.

4.1.2. Daya Bay The Daya Bay experiment [20] will receive neutrinos from three nuclear plants, each consisting of two cores: Daya Bay, Ling Ao I and Ling Ao II (scheduled to be commissioned by the end of 2010) located in the south of China, 55 km to the northeast of Hong Kong. The thermal power of each core is 2.9 GW, hence the existing total thermal power is 11.6 GW, and will be 17.4 GW after 2010.

The basic experimental layout of Daya Bay consists of three underground experimental halls, one far and two close, linked by horizontal tunnels under construction. The geometry of the reactor cores, the two near detector stations and the far detector station is illustrated in fig. 7. It is evident from this configuration that

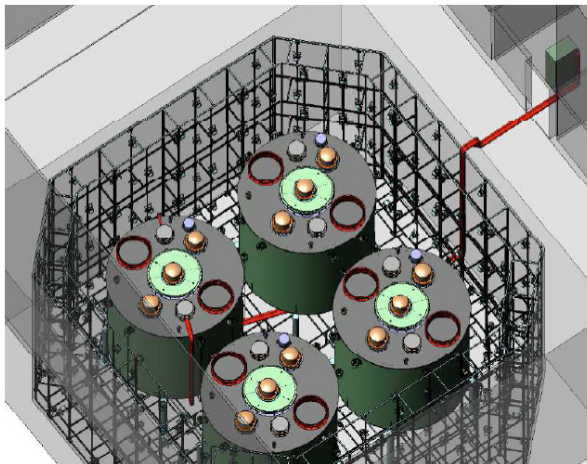


Figure 8. A drawing of the Daya Bay far detector hall showing the four detectors in a water pool instrumented with PMTs to detect cosmic muons. From [20].

the flux measured by the near detectors will not be identical to the one seen by the far detector. Each close detector hall, at a depth of about 100 m.w.e., will host two 20 ton gadolinium doped (0.1%) liquid scintillator detectors, while the far hall, 350 m.w.e., will host four such detectors. The detectors are designed to be movable so that the close detectors and the far ones can be swapped. This swapping is not necessary to reach the designed systematics (0.38%), but could be performed to cross check the sensitivity and possibly further reduce the systematic errors (down to 0.18%).

The design of the detectors is very similar to the Double Chooz one, with the notable difference that the three stations will be submerged in a water pool of 2.5 m depth to shield the detectors from ambient radiation and spallation neutrons. Above the pool a muon tracking detector made of 4 layers of resistive-plate chambers (RPCs) will be installed.

4.1.3. Reno The RENO [22] experiment is located on the site of the Yonggwang nuclear power plant in the southwestern part of Korea. The plant consists of six reactors lined up in roughly equal distances and spans about 1.3 km. With a total thermal power of 16.4 GW it is at present the second largest nuclear reactor plant in the world.

RENO will use two identical detectors, a close detector at about 290 m from the reactor array (at a depth of about 110 m.w.e.) and a far detector at 1380 m (at a depth of about 450 m.w.e.), see fig. 7. The design of the RENO detectors is very similar to Double Chooz, the active target will be 15.5 ton of Gd loaded (0.1%) liquid scintillator. The outer veto system is a layer of water, 1.5 m thick, contained in a 30 cm thick concrete vessel. PMTs are mounted on the inner surface of the veto container for detecting Čerenkov light from cosmic muons. Goal of the experiment is to reach a $< 0.5\%$ systematic error.

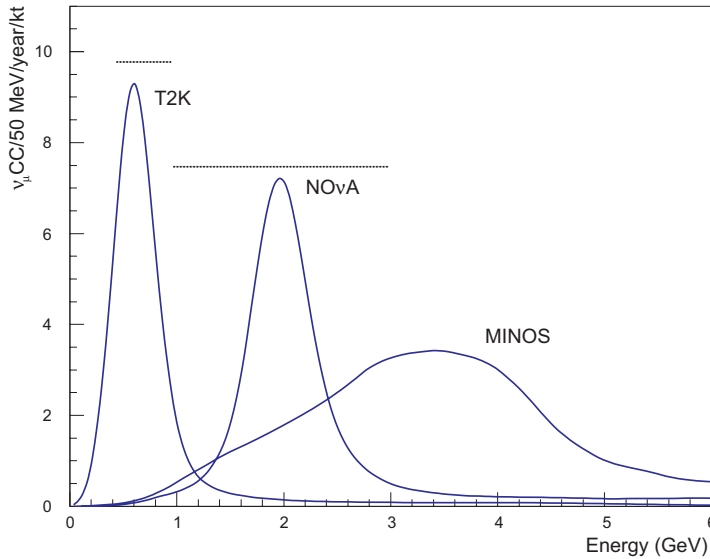


Figure 9. Muon neutrino interaction rates in MINOS, NO ν A, and T2K assuming no oscillations, normalised to one year of operation at the power of 410, 700, and 750 KW, respectively. The horizontal dotted lines represent the neutrino energy region where the $\nu_\mu \rightarrow \nu_e$ oscillation probability is bigger than 50% of the maximum ($\delta = 0$ and normal hierarchy). The MINOS probability is very similar to NO ν A.

4.2. Accelerator experiments

Accelerator experiments look for the appearance of the ν_e flavour in an almost pure ν_μ beam, due to oscillations. The background rate has an intrinsic component given by the ν_e contamination in the neutrino beam, ranging from 0.5% to 1%. Detector backgrounds can be generated by NC events where a π^0 produces a signal misidentified as an electron, or ν_μ CC events where the muon is misidentified as an electron.

Several experiments already tried in the past to detect $\nu_\mu \rightarrow \nu_e$ transitions at accelerators with short baselines. The most stringent result comes from the NOMAD experiment that reached a sensitivity on the probability of these transitions $P(\nu_\mu \rightarrow \nu_e) \leq 0.7 \cdot 10^{-3}$ (90% CL) [154]. The challenge of the next generation of long baseline experiments is to obtain similar sensitivities with detectors 10^4 more massive than the NOMAD detector [155], a 3 ton, low density (0.1 g/cm^3), very sophisticated spectrometer. The pioneering $\nu_\mu \rightarrow \nu_e$ long-baseline appearance searches have been performed by the K2K [131] and MINOS [19] experiments, see section 3.4.

A rough estimate for the sensitivity can be obtained by comparing the signal to the statistical and systematical uncertainty of the background:

$$\frac{S}{\sqrt{B + \sigma_{\text{bg}}^2 B^2}}, \quad (26)$$

where S (B) is the number of signal (background) events, and σ_{bg} is the uncertainty in the background.

It is almost impossible to derive a general rule for the number of events in the far

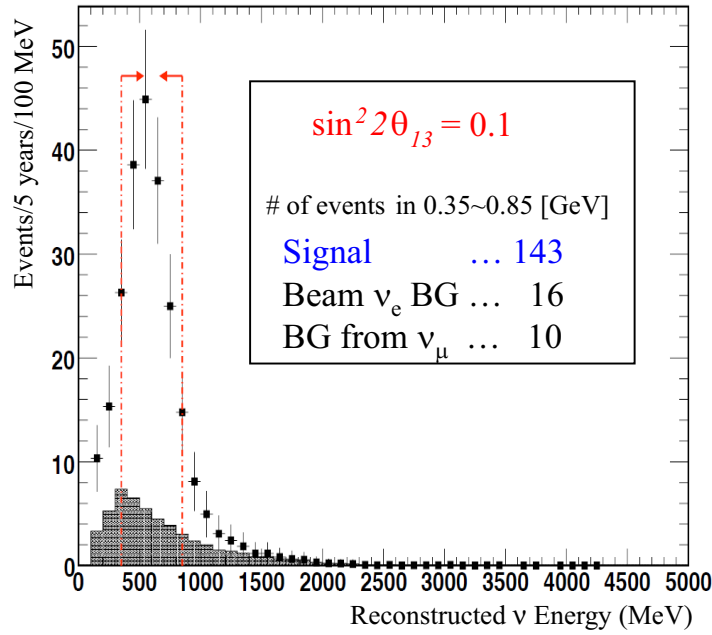


Figure 10. Signal and backgrounds events for T2K, computed for $\sin^2 2\theta_{13} = 0.1$, $\delta = 0$, $\Delta m_{31}^2 = 3 \cdot 10^{-3} \text{ eV}^2$ and normal hierarchy. From [156].

detector, since it depends very much on the geometry of the target, the optics of the neutrino beam line, and the off-axis angle. The number of signal events S is proportional to the detector mass times the power of the primary proton beam. Surprisingly enough S does not depend very much on the primary proton energy and on the baseline L assuming the far detector at the first oscillation maximum. This implies a constant value of L/E with E the neutrino energy. Since the neutrino cross section generally increases as E^r with $r \simeq 1 - 2$, the $1/L^2$ scaling of the beam flux is largely compensated. A comparison of the neutrino interaction rates in T2K, NO ν A and MINOS is reported in fig. 9.

The SuperKamiokande water Čerenkov detector used in T2K already demonstrated to be capable of keeping detector backgrounds to a level smaller than the intrinsic ν_e contamination of conventional neutrino beams. Also the total active scintillator technology (TASD) chosen for NO ν A allows to keep beam and detector backgrounds at comparable level. As an example of signal and background events in an accelerator experiment we reproduce signal and background events in T2K as shown in [156].

However, the water Čerenkov and TASD techniques allow a reasonable event energy reconstruction only for quasi-elastic (QE) neutrino interactions. QE interactions produce just one charged particle above the Čerenkov threshold, resulting in just one Čerenkov ring in the detector. The two-body kinematics allows a precise reconstruction of the incident neutrino energy from the measured momentum of the outgoing lepton and the known direction of the incoming neutrino. E.g., for a QE ν_μ event one has

$$E_\nu^{\text{rec}} \simeq \frac{1}{2} \frac{(M_p^2 - m_\mu^2) + 2E_\mu M_n - M_n^2}{-E_\mu + M_n + p_\mu \cos \theta_\mu} \quad (27)$$

where M_p , M_n , m_μ , E_μ , p_μ , $\cos\theta_\mu$ are the proton, neutron, muon masses, muon energy, momentum and angle with respect to the incoming neutrino direction. Single ring events produced by non-QE interactions could bias the energy reconstruction because in their case the two body kinematics does not hold. For this reason it is important to precisely know the non-QE/QE ratio in the neutrino interactions.

Other detector technologies, such as liquid argon TPCs, could suppress detector backgrounds to a negligible level and efficiently reconstruct neutrino interaction events of any multiplicity, and are very promising for future neutrino oscillation experiments.

A beam configuration used to optimise long baseline experiments with the goal of measuring θ_{13} is the off-axis configuration, a concept that was firstly proposed in [157]. According to the two-body π -decay kinematics, all the pions above a given momentum produce neutrinos of similar energy at a given angle $\theta \neq 0$ with respect to the direction of the parent pion (contrary to the $\theta = 0$ case where the neutrino energy is proportional to the pion momentum).

An off-axis configuration offers several advantages for a long baseline experiment optimised to detect sub-leading $\nu_\mu \rightarrow \nu_e$ oscillations. First, the off-axis neutrino flux at the desired energy is higher than in an on-axis configuration. Second, the neutrino flux at higher energies than the oscillation maximum is greatly reduced, with a consequent reduction of backgrounds due to π^0 generated by neutral current events. Both of these effects are clearly visible in comparing the MINOS (on-axis) and NO ν A (off-axis) spectra in fig. 9. Third, the intrinsic background due to beam ν_e is less around the oscillation maximum (about 0.4% in T2K) since ν_e are mostly generated by three body meson decays that have different kinematics than the two body pion decays. These advantages overcompensate the smaller total neutrino flux (even when multiplied by the oscillation probability) of the off-axis configuration.

In an appearance experiment the influence of systematic errors is very much reduced if compared to the reactor experiments. Nevertheless a close detector is necessary in order to precisely measure the flux of ν_μ , that are going to oscillate into ν_e in the far detector, to measure interaction cross sections of signal and background processes, and to measure the backgrounds for the signal ν_e . As extensively discussed in [158] the task of the close detector is not just a background subtraction, since for instance, factors as the QE/non-QE ratio can spoil the experimental sensitivity. As it will be described in the following the T2K experiment renounced to have a replica of the far detector in the close position, and designed a very sophisticated close detector capable of precisely measuring the exclusive neutrino cross sections that play a role in the signal and backgrounds in the far detector as well as the flux of ν_μ . NO ν A instead is planning to have just a replica of the far detector in the close station, but it shouldn't be missed the fact that in the same beam line (on-axis) will soon operate experiments specialised in measuring neutrino cross sections, like MINER ν A [159].

4.2.1. T2K The T2K (Tokai-to-Kamioka) experiment [24] will use a high intensity off-axis (2.5°) neutrino beam, with a peak energy of 700 MeV, generated by a 30 GeV

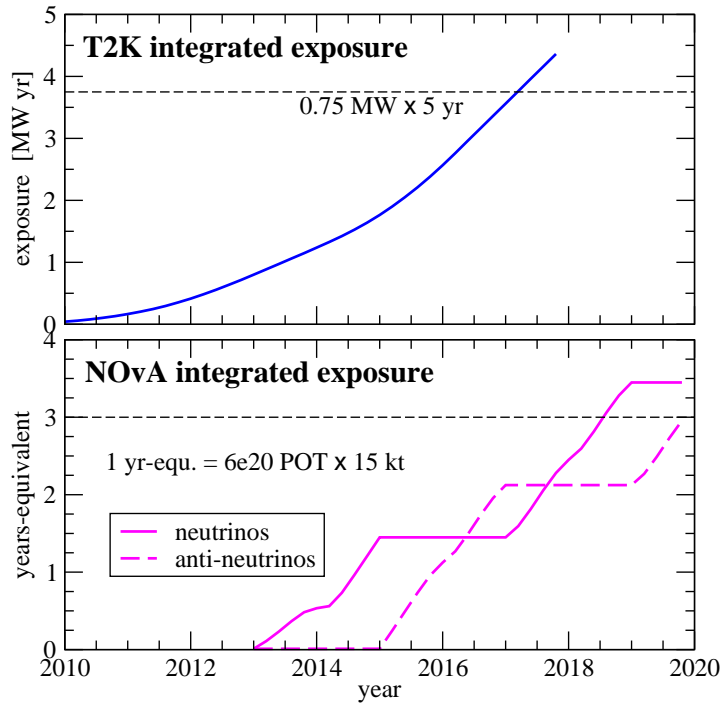


Figure 11. Integrated exposures for the T2K (top) and NOνA (bottom) experiments. The T2K beam power plan is based on [156]. The NOνA exposure has been normalised to nominal “NOνA years”, which corresponds to 6×10^{20} protons-on-target (pot) and a 15 kt detector. The shown curves take into account the plan for the available detector mass as a function of time, as well as the available pot [160].

proton beam at J-PARC (Japan Proton Accelerator Research Complex) fired to the SuperKamiokande detector, located 295 km from the proton beam target. The design intensity of the J-PARC proton beam is $3.3 \cdot 10^{14}$ protons/pulse with a repetition rate of 3.3 s, corresponding to a beam power of about 750 kW. The experiment is expected to collect data for about 10^7 s/year, performances are normalised to a 5 year run at the nominal power. Fig. 11 shows the integrated exposure as a function of time using the expected beam power shown in [156]. According to this plan, the nominal exposure will be reached around 2017.

The schematic view of the T2K neutrino beam line is shown in fig. 12 (left). The primary proton beam interacts in a helium-cooled graphite target placed inside the first horn. The beam optics includes three horns running at 320 kA with a maximum magnetic field of 2.1 T. The decay volume is 94 m long after the target region with a variable cross section starting at 2.2 m (W) at 2.8 m (H) and increasing to 3.0 m at 4.6 m at the far end, filled with inert helium gas held at 1 atm. A beam dump, constructed of cooled graphite and copper blocks is placed at the end of the decay volume.

A sophisticated near detector complex has been built at a distance of 280 m from the target. This complex has two detectors: one on-axis (INGRID) and the other off-axis (ND280). This off-axis detector (fig. 12, right) is a spectrometer built inside the magnet of the former experiments UA1 and NOMAD, operating with a magnetic

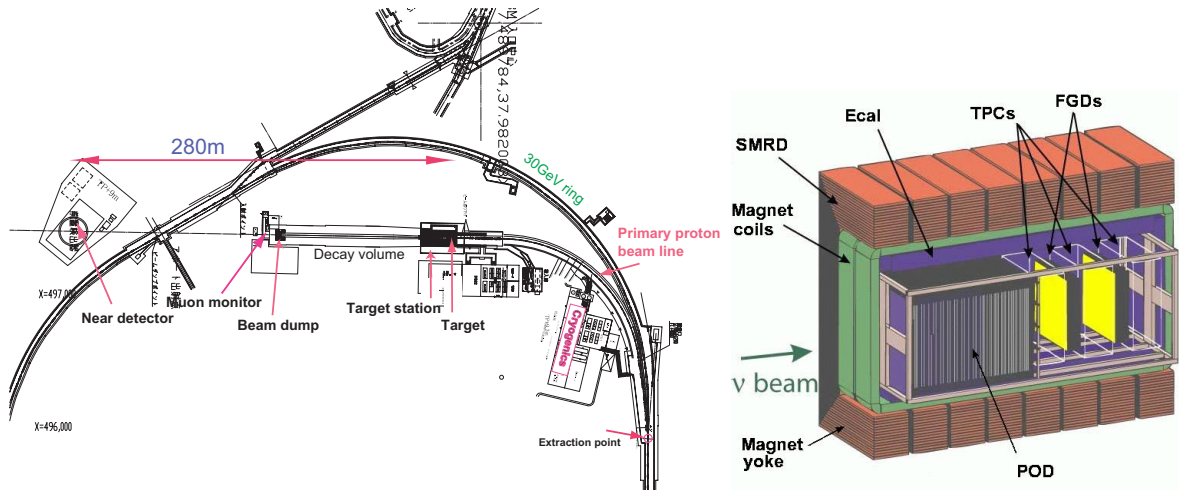


Figure 12. Left: the layout of the T2K beam line, showing the location of primary proton beam line, target station, decay volume, beam dump, muon monitors and near neutrino detectors, [161]. Right: sketch of the T2K ND280 off-axis near detector.

field of 0.2 T. It includes a Pi-Zero detector (POD), a tracking detector made by three time projection chambers (TPCs) and two fine grained scintillator detectors (FGDs) acting as an active target, a 4π electromagnetic calorimeter (Ecal), and a side muon range detector (SMRD). To reduce systematic errors both the POD and the FGDs incorporate water targets (the same material of the far detector). Neutrino rates in the close detector will be about $160000 \nu_\mu$ ($3200 \nu_e$) interactions/ton/yr at the nominal beam intensity of $0.75 \text{ MW} \cdot 10^7 \text{ s}$.

ND280 is expected to calibrate the absolute energy scale of the neutrino spectrum with 2% precision, measure the non-QE/QE ratio at the 5-10% and monitor the neutrino flux with better than 5% accuracy. The momentum resolution of muons from the charged current quasi-elastic interactions (CCQE) should be better than 10%. The ν_e fraction should be measured with an uncertainty better than 10%. A measurement of the neutrino beam direction, with a precision better than 1 mrad, is required from the on-axis detector.

The close detector location, 280 m from the target, is too close to the decay tunnel to have a neutrino flux identical to the far detector flux. Indeed differences as big as 50% are expected between the two fluxes, reducing the capability of the close detector of reducing systematic errors independently from any Monte Carlo simulation. A more distant close detector station could attenuate the near-far neutrino flux differences, but for the moment is not foreseen by the experiment.

A fundamental tool to better control the neutrino flux is the ongoing measurement of the hadro-production in a T2K target replica by 30 GeV protons by the NA61 experiment at CERN [162]. Following the successful example of the measurements done by the HARP experiment [163] for the K2K [164] and for the MiniBooNE [165] targets, NA61 data should greatly improve the accurateness of the neutrino beam line simulation.

Signal events are detected by the SuperKamiokande detector with an efficiency of

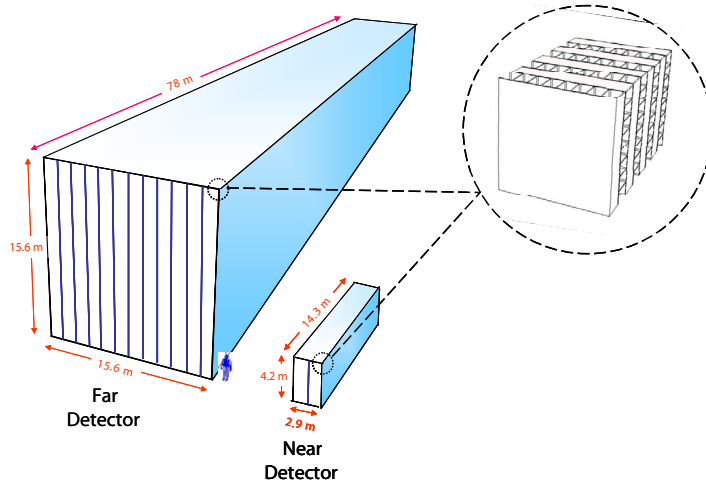


Figure 13. Sketch of the $\text{NO}\nu\text{A}$ detectors. The insert figure shows the plane arrangement of each detector. From [166].

45% and with a detector background contamination smaller than the intrinsic beam ν_e contamination (roughly in the 2:3 ratio, see also fig. 10).

4.2.2. $\text{NO}\nu\text{A}$ The $\text{NO}\nu\text{A}$ experiment [23] will run at an upgraded NuMI neutrino beam expected to deliver $6.5 \cdot 10^{20}$ pot/year, corresponding to a beam power of 700 kW, generating a neutrino beam with an average energy $E_\nu \sim 2$ GeV and a ν_e contamination less than 0.5%.

The far detector, placed at baseline of 810 km, 14 mrad (0.8°) off-axis, will be a “totally active” tracking liquid scintillator, constructed from liquid scintillator contained inside extruded PVC cells. Each cell is 3.9 cm wide by 6.0 cm deep and is 15.5 meters long, they will be arranged in an alternating plane structure composed of vertical and horizontal cells. Scintillation light will be guided to APD photo-detectors using wavelength shifting fiber. $\text{NO}\nu\text{A}$ will be located near Ash River and will have a total mass of 15 kilotons (385000 cells) and be 15.7 meters wide, 15.7 meters tall, 78 meters long (the only non-cylindrical detector in this generation of experiments). It will run on surface, with a modest overburden of 3 m of concrete. It is expected to detect ν_e signals with an efficiency of 26% (including acceptance) and to reduce the detector background rate to a level comparable to the rate from the intrinsic beam ν_e contamination. The close detector will be a 215 ton replica of the far detector, placed 14 mrad off the NuMI beam axis at a distance of 1 km from the target. A sketch of the $\text{NO}\nu\text{A}$ detectors is shown in fig. 13.

$\text{NO}\nu\text{A}$ plans to alternate between neutrino mode and antineutrino mode: the focus of the experiment is to provide data on the neutrino mass hierarchy, where $\text{NO}\nu\text{A}$ has a clear advantage with respect to T2K thanks to the longer baseline, see e.g. [167] for a recent sensitivity study, and [168–170] for discussions of the T2K/ $\text{NO}\nu\text{A}$ complementarity/synergy. A possible scenario [160] on the time evolution of neutrino

and antineutrino exposure is shown in fig. 11, which takes into account the build-up of the detector mass as well as the available beam power. As a second phase, the NuMI beam intensity could be increased to 1.2 MW (“SNUMI”) or to 2.3 MW (“Project X”) in case the new proton driver of 8 GeV/c and 2 MW will be built at FNAL.

5. Phenomenology and sensitivity estimates for upcoming experiments

5.1. Complementarity of reactor and superbeam experiments

A natural classification of the 5 upcoming experiments is the distinction between reactor and accelerator (superbeam) experiments. Apart from the vastly different experimental configurations and challenges (see section 4) there is also an important difference from the point of view of oscillation physics. While reactor experiments search for the disappearance of electron antineutrinos, accelerator experiments look for the appearance of electron (anti)neutrinos in a beam initially composed mainly of muon (anti)neutrinos.

Let us now discuss the relevant oscillation probabilities. We denote with L, E_ν, V the distance from the neutrino source and the detector, the neutrino energy, and the matter potential, respectively, with $V = \sqrt{2}G_F N_e$ where N_e is the electron density along the neutrino path. Furthermore we introduce the abbreviations

$$\Delta \equiv \frac{\Delta m_{31}^2 L}{4E}, \quad A \equiv \frac{2EV}{\Delta m_{31}^2}, \quad \alpha \equiv \frac{\Delta m_{21}^2}{\Delta m_{31}^2}. \quad (28)$$

Note that the signs of all three of these quantities depend on the neutrino mass hierarchy encoded in the sign of Δm_{31}^2 .

In the case of reactor experiments with $L \lesssim 2$ km the matter effect is negligible and the survival probability is given by

$$P_{ee} \approx 1 - \sin^2 2\theta_{13} \sin^2 \Delta - \alpha^2 \Delta^2 \sin^2 2\theta_{12}. \quad (29)$$

As mentioned in the discussion of the CHOOZ experiment in section 3.1, the last term due to Δm_{21}^2 is suppressed by the small solar mass squared difference and can be neglected as long as $\sin^2 2\theta_{13} \gg \alpha^2 \simeq 10^{-3}$, and in this case P_{ee} is independent of the solar parameters θ_{12} and Δm_{21}^2 . Furthermore, the survival probability eq. 29 does neither depend on θ_{23} , on the CP phase δ , nor on the sign of Δm_{31}^2 . Hence reactor experiments provide a “clean” measurement of θ_{13} , free of correlations with other parameters, apart from $|\Delta m_{31}^2|$, which, however, is relatively precisely known [151, 152].

Let us now move to long-baseline appearance experiments. For typical neutrino energies in the GeV range and baselines larger than 100 km one cannot neglect the matter effect. However, for baselines smaller than a few 1000 km it is a good approximation to assume a constant matter density, given by the average density along the neutrino path. In that case a rather useful expression for the $P_{\nu_\mu \rightarrow \nu_e} \equiv P_{\mu e}$ appearance probability can be obtained by considering terms up to second order in the small quantities s_{13} and α [171–173]:

$$P_{\mu e} \approx \sin^2 2\theta_{13} s_{23}^2 \frac{\sin^2(A-1)\Delta}{(A-1)^2}$$

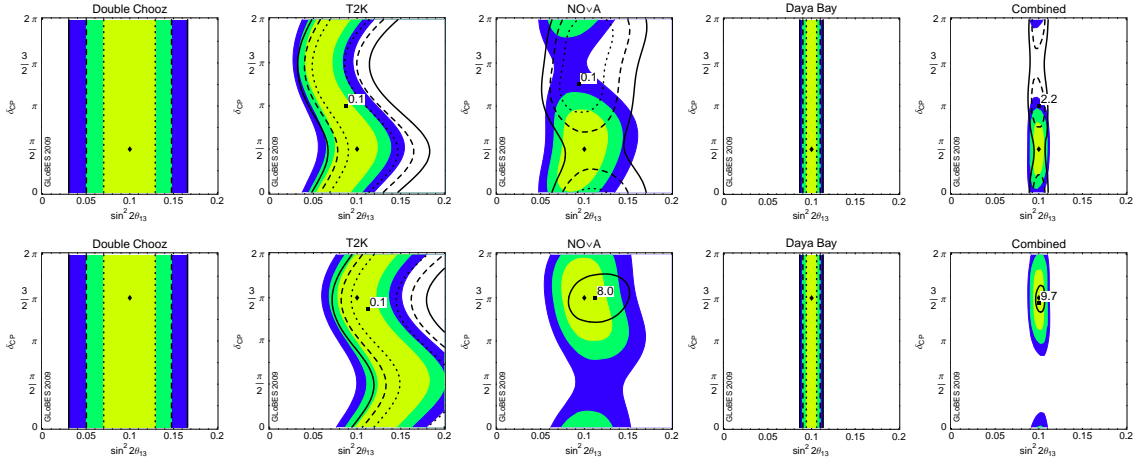


Figure 14. Exemplary fit results for Double Chooz, T2K, NO ν A, Daya Bay, and the combination. Shown are fits in the θ_{13} - δ plane assuming $\sin^2 2\theta_{13} = 0.1$ and $\delta = \pi/2$ (upper row) and $\delta = 3\pi/2$ (lower row). A normal simulated hierarchy is assumed. The contours refer to 1σ , 2σ , and 3σ (2 dof). The fit contours for the right fit hierarchy are shaded (coloured), the ones for the wrong fit hierarchy are shown as curves. The best-fit values are marked by diamonds and boxes for the right and wrong hierarchy, respectively, where the minimum χ^2 for the wrong hierarchy is explicitly shown. Reprinted from Ref. [167], Copyright (2009), with permission from JHEP.

$$\begin{aligned}
 & + \alpha \sin 2\theta_{13} \sin 2\theta_{12} \sin 2\theta_{23} \cos(\Delta + \delta) \frac{\sin A\Delta}{A} \frac{\sin(A-1)\Delta}{A-1} \\
 & + \alpha^2 \sin^2 2\theta_{12} c_{23}^2 \frac{\sin^2 A\Delta}{A^2}. \quad (30)
 \end{aligned}$$

This equation holds for neutrinos; for anti-neutrinos change $\delta \rightarrow -\delta$ and $V \rightarrow -V$. The term in the first line of eq. 30 is similar to a two-flavour oscillation probability, apart from the s_{23}^2 factor which controls the fraction of the ν_μ flavour participating in the $\nu_e - \nu_\mu$ oscillations. This term dominates for large θ_{13} . The term in the second line of eq. 30 corresponds to an interference term between oscillations with Δm_{31}^2 and Δm_{21}^2 . It depends on the CP phase δ and is responsible for CP violation. The term in the last line is independent of θ_{13} and describes oscillations with Δm_{21}^2 . It can be neglected for $\sin^2 2\theta_{13} \gtrsim 0.01$.

Obviously, the parameter dependence of the appearance probability is much more complicated than the one for disappearance in reactor experiments, as it depends on all 6 oscillation parameters. If information on θ_{13} is to be extracted from an appearance measurement the correlations with the parameters δ and $\text{sgn}(\Delta m_{31}^2)$ are especially important [174]. The difference between reactor and super beam experiments is illustrated in fig. 14, taken from [167]. It shows how typical fits in the θ_{13} - δ plane would look like if θ_{13} was large ($\sin^2 2\theta_{13} = 0.1$) and δ was close to maximal CP violation $\delta = \pi/2$ (upper rows) and $\delta = 3\pi/2$ (lower rows). Here NH has been assumed to generate the “data”. Using this “true” hierarchy in the fit, the coloured regions are obtained. When the data is fitted with the “wrong” hierarchy, i.e., with IH in this case, the regions

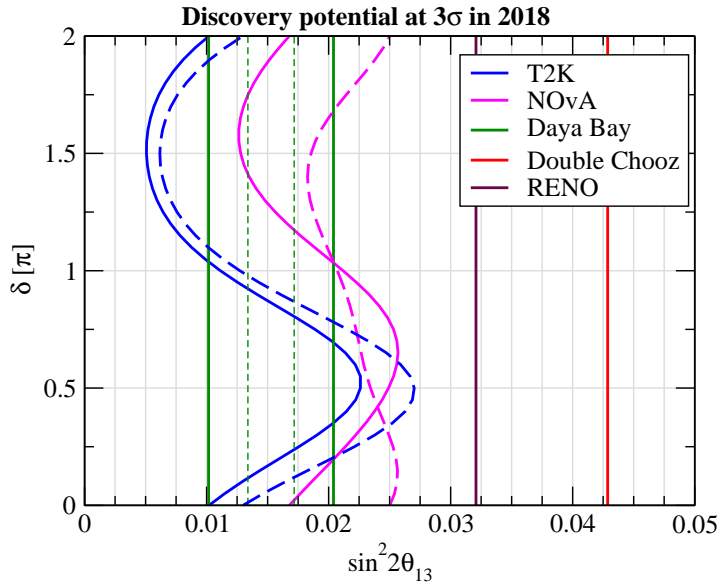


Figure 15. Discovery potential of the five upcoming experiments in the plane of $\sin^2 2\theta_{13}$ and δ expected in 2018, see section 5.3 for our assumptions on exposure. To the right of the curves a non-zero value of θ_{13} can be established at 3σ . For the beam experiments we show normal (solid) and inverted (dashed) hierarchies, while reactor experiments are independent of the hierarchy. The four lines for Daya Bay correspond to different assumptions on the achieved systematic uncertainty, from weakest to strongest sensitivity: 0.6% correlated among detector modules at one site, 0.38% correlated, 0.38% uncorrelated among modules, 0.18% uncorrelated.

delimited by the curves are obtained.

The figures show the characteristics of the different classes of experiments: The reactor experiments do not depend on δ , and the wrong fit hierarchy coincides with the right hierarchy. For T2K, which is simulated with neutrino running only, there is some dependence on δ , but the correlation between δ and θ_{13} cannot be resolved. We observe the typical S-shape of the allowed regions, emerging from the $\cos(\Delta + \delta)$ term in eq. 30. The wrong hierarchy contours are slightly shifted, but the minimum χ^2 is close to zero. $\text{NO}\nu\text{A}$, on the other hand, has both neutrino and anti-neutrino running in the simulation, which means that the correlation can, at least in principle, be resolved. The wrong hierarchy can in some cases be excluded because of larger matter effects. In the combination of the experiments, the combination between Daya Bay and the beams allows for a substantial reduction of the allowed parameter space due to almost orthogonal measurements [151, 152, 175]. In the most optimistic cases, the mass hierarchy can be determined at 3σ confidence level, and maximal CP violation can be established at relatively modest confidence as well. However, note that these optimistic cases represent only a very small fraction of the parameter space, see [167] for a discussion of the possibilities to measure CP violation and the mass hierarchy with these experiments.

Fig. 15 shows the θ_{13} discovery reach of the five upcoming experiments expected

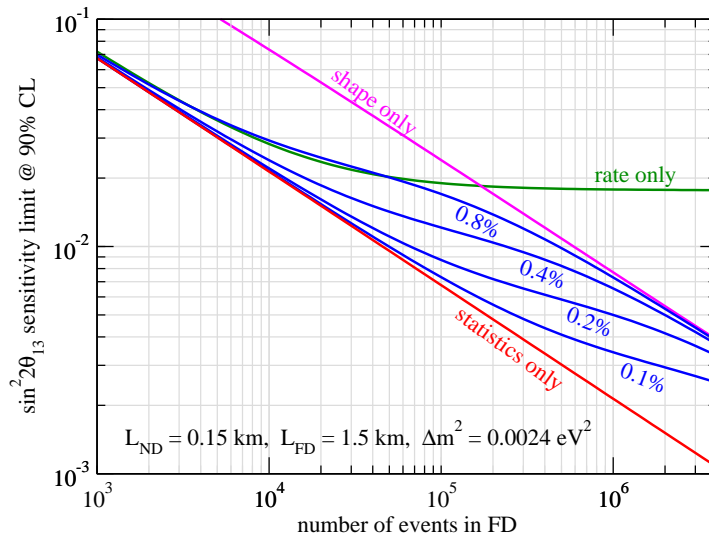


Figure 16. Illustration of the luminosity scaling of the $\sin^2 2\theta_{13}$ sensitivity at 90% CL of a fictitious reactor experiment. The horizontal axis shows the number of events in the far detector at a distance of 1.5 km from the reactor. We show the sensitivity for statistical errors only (red), as well as various values for the relative normalisation uncertainty between near and far detectors (blue curves with labels). The magenta and green curves show the sensitivity obtained for using only shape and only rate information, respectively.

in 2018. Details about our exposure assumptions are given in section 5.3. It is clear from the figure that the discovery potential of the appearance experiments strongly depends on the CP-phase as well as on the neutrino mass hierarchy. We observe that the inverted hierarchy gives a weaker sensitivity. Hence, in case no appearance signal is found the final θ_{13} limit will be set by the IH. Note that this is completely analogous to the present information on θ_{13} from the MINOS ν_e appearance data, compare figs. 15 and 3 (left). The fact that the IH has a weaker sensitivity is a consequence of the matter effect. It can be understood by considering the $(A - 1)$ terms in eq. 30. Since MINOS as well as T2K operate only with neutrinos we have $V > 0$, and A is positive (negative) for NH (IH). Hence, for NH (IH) the factors $(A - 1)$ in the denominator lead to enhancement (suppression) of the oscillation probability, and therefore IH gives a weaker limit. The different shape of the IH curve for $\text{NO}\nu A$ results from the anti-neutrino running included in the $\text{NO}\nu A$ run plan. As evident from the figure, reactor experiments are neither sensitive to the value of δ nor to the mass hierarchy.

5.2. On statistical errors and systematical uncertainties

Apart from the differences in the oscillation physics between reactor and super beam experiments there is also an important difference in how statistical and systematic errors influence the final sensitivity.

Fig. 16 shows the sensitivity to $\sin^2 2\theta_{13}$ as a function of the number of events for various assumptions on systematical uncertainties for a fictitious reactor experiment

with one reactor core and two detectors, at 0.15 and 1.5 km. The statistics-only sensitivity displays the expected $1/\sqrt{N}$ scaling. The blue curves correspond to different values of the relative normalisation uncertainty between the two detectors. Turning on this uncertainty deteriorates the sensitivity above a characteristic exposure. Remarkably, at very high exposures again a $1/\sqrt{N}$ scaling is recovered [152]. This is a consequence of the information coming from the shape of the spectrum. The magenta line in the figure shows the limit from only shape information, with leaving the total number of events unconstrained in the fit. In reality also the spectral shape will suffer from some systematical uncertainty, which at some point will cut off again the $1/\sqrt{N}$ scaling, see e.g., Refs. [138, 152] for a discussion. If only the total rate without any spectral information is used, the final sensitivity is just given by the overall normalisation uncertainty, as illustrated by the green curve in fig. 16. To get a feeling about the three reactor experiments Double Chooz, RENO, and Daya Bay in relation with fig. 16 we recall the expected events per year given in tab. 2 as $(1.5, 3, 10) \times 10^4$, respectively. Note, however, that the figure is for a fixed far detector baseline of 1.5 km and one single reactor, which does not correspond to any of the three experiments, and therefore the figure cannot be applied exactly to the specific experimental configurations.

We note that especially the high-statistics experiment Daya Bay, with let's say 3×10^5 events after 3 years, is quite sensitive to the achieved systematic. This is illustrated in fig. 15, where we show the Daya Bay sensitivity for different choices on systematics. The four lines correspond to various assumptions on the relative normalisation uncertainty of the 8 detector modules. For the most conservative limit we assume the same uncertainty as claimed by Double Chooz, 0.6%, and take this error correlated between detector modules at each detector site. The Daya Bay “baseline” systematics is 0.38%. The two dashed curves correspond to this value assuming it either correlated or uncorrelated among detector modules at one site. The most aggressive curve shown in fig. 18 assumes the “goal” value of the systematics of 0.18%, uncorrelated between all detector modules. Let us stress that of course systematics are also crucial for Double Chooz and RENO. In those cases we have adopted a systematical error of 0.6%, as stated in the proposals. The final Double Chooz and RENO sensitivities will depend in a similar way on the assumed systematics value as exemplary shown for the case of Daya Bay in the plot.

Let us now discuss the impact of systematics and statistics on the θ_{13} measurement in super beam experiments. As an example we consider a slightly modified version of the T2K experiment, where, e.g., both neutrino and anti-neutrino running is assumed with a ratio of 1:3. A detailed description can be found in [158]. Fig. 17 (left) shows the smallest value of $\sin^2 2\theta_{13}$ which can be distinguished from $\theta_{13} = 0$ as a function of the luminosity, assuming two representative values for the CP phase which correspond roughly to the best and worst sensitivity. The first observation is that for an exposure corresponding roughly to the nominal T2K exposure (marked by the vertical line labeled “T2K”) systematics have only a small impact, since this measurement is largely dominated by statistics. Numerically, the sensitivity at a T2K exposure decreases

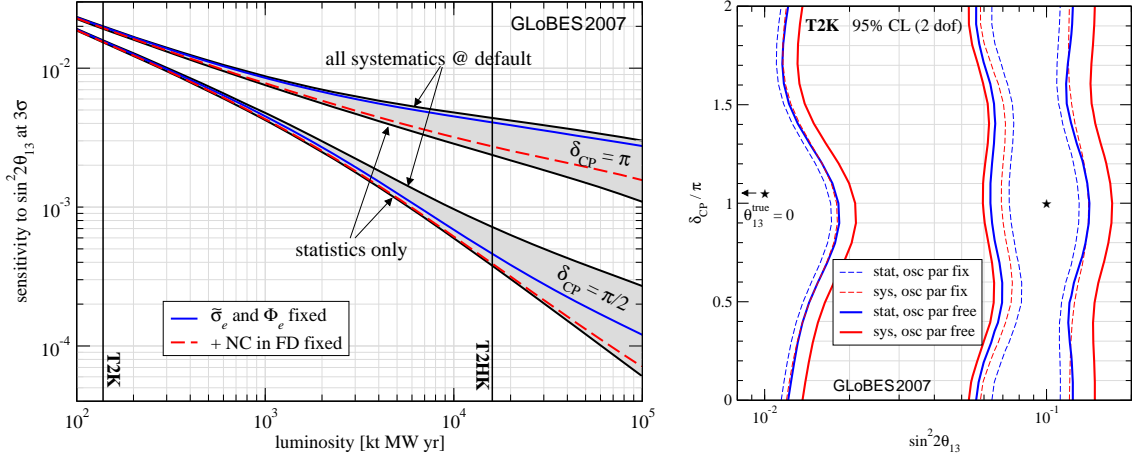


Figure 17. Left: Sensitivity to a non-zero θ_{13} for a T2K-like experiment as a function of exposure for $\delta = \pi/2$ and π for a default choice of systematical errors and for statistical errors only (curves delimiting the shaded region). Furthermore, the sensitivity obtained without uncertainty on the intrinsic beam background (blue) and without an uncertainty on the NC background in the far detector (red-dashed) is shown. Right: Allowed region in the plane of $\sin^2 2\theta_{13}$ and δ for two example choices for the input values marked by stars in the figure. Allowed regions are shown for all combinations of statistical errors only, systematics included, all other oscillation parameters fixed, and free (where for the solar parameters present errors are assumed). The sign(Δm_{31}^2) degeneracy is neglected, and $\theta_{23}^{\text{true}} = \pi/4$. Reprinted from Ref. [158], Copyright (2008), with permission from JHEP.

from $\sin^2 2\theta_{13} = 0.0167$ to 0.0172 for $\delta = \pi/2$, and from $\sin^2 2\theta_{13} = 0.0206$ to 0.0214 for $\delta = \pi$.

Only for much larger exposures systematics have a non-negligible impact on the θ_{13} discovery reach. According to the discussion related to eq. 26, the uncertainty on the background is the most relevant systematics. Its impact is controlled by the ability of the near detector to predict the background in the far detector. Fig. 17 shows also curves assuming a perfectly known ν_e beam background, and no uncertainty at all on the background (*i.e.*, fixing the ν_e beam contamination as well as the NC background). If the total background is fixed the sensitivity is close to the pure statistics case. It is interesting to note that for the two examples of δ shown in the figure the importance of beam and NC backgrounds is different. This is an effect of the spectral shapes of the signal relative to the background, since the spectrum of the signal depends on the value of δ , and also beam and NC backgrounds have rather different shapes.

Fig. 17 (right) shows the allowed region in the space of $\sin^2 2\theta_{13}$ and δ obtained by the same modified T2K-like configuration. The impact of systematics is small, though not negligible in this case. Furthermore, we observe that the uncertainty on the other oscillation parameters has a sizable impact on the allowed region. This effect comes entirely from the atmospheric parameters Δm_{31}^2 and θ_{23} . Apparently the disappearance

|| Note the different shapes of the regions from fig. 17 (right) and the corresponding panels of fig. 14. The reason is the anti-neutrino running assumed for fig. 17.

channel does not provide enough accuracy on these parameters to avoid an effect on the θ_{13} determination. For the solar parameters the accuracy from present data is sufficient to eliminate any effect on the results shown in the figure.

5.3. Sensitivity predictions for the upcoming experiments

We now discuss the sensitivity of the different experiments to θ_{13} , using two different performance indicators: the θ_{13} sensitivity limit and the θ_{13} discovery potential. The θ_{13} sensitivity limit describes the ability of an experiment to constrain θ_{13} if no signal is seen. It is basically determined by the worst case parameter combination which may fake the simulated $\theta_{13} = 0$. The sensitivity limit does not depend on the simulated hierarchy and δ , as $\theta_{13} = 0$ is used to calculate the fake data. For a more detailed discussion, see appendix C of [138]. The θ_{13} discovery potential is given by the smallest true value of $\theta_{13} > 0$ which cannot be fitted with $\theta_{13} = 0$ at a given CL. Since the simulated θ_{13} , δ , and hierarchy determine the simulated rates, the θ_{13} discovery potential will depend on the values of all these parameters chosen by nature. On the other hand, correlations and degeneracies are of minor importance because for the fit $\theta_{13} = 0$ is used.

For reactor experiments both measures (sensitivity limit and discovery potential) are very similar, since statistics are Gaussian and the oscillation physics is simple. For beam experiments the smallest θ_{13} discovery potential for all values of δ and mass hierarchies (risk-minimised θ_{13} discovery potential) is often similar to the θ_{13} sensitivity limit. However, notable deviations from this rule occur due to Poisson statistics as well as more complicated oscillation physics implying correlations and degeneracies. In particular, we find that for low exposures the worst case discovery potential of the beams is somewhat better than the limit in case of no signal at the same confidence level.

We are going to show the evolution of the θ_{13} sensitivity with time, assuming the following schedules for the experiments based on up-to-date information. For Double Chooz the far detector starts data taking in June 2010, while near detector data will become available beginning of 2012. RENO starts data taking with both close and far detectors end of 2010. For Daya Bay we do not consider the periods where only the near detectors are available in 2011, but consider the start of the full experiment with all detectors at the end of 2011. For all reactor experiments we assume that all reactors are at nominal power all time according to the event numbers per year given in table 2. For T2K and NO ν A we use the exposures as a function of time shown in fig. 11, assuming that protons on target are uniformly distributed along the year, not taking into consideration the specific schedules of the accelerators. In all cases we assume that results are available instantaneously with data.

The simulations of T2K and NO ν A are performed with the GLoBES software [133, 134] based on the experiment definitions developed in [167] and available at the GLoBES web-page. Modifications to the T2K simulation have been introduced due to recent updates on efficiencies (it now reproduces fig. 10). For the reactor experiments an independent code has been developed, allowing for an arbitrary number of reactors and

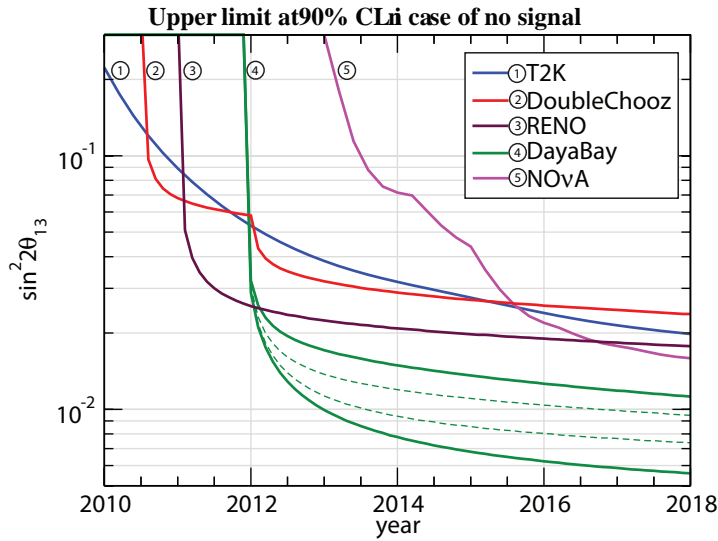


Figure 18. Evolution of the θ_{13} sensitivity limit as a function of time (90% CL), i.e., the 90% CL limit which will be obtained if the true θ_{13} is zero. The four curves for Daya Bay correspond to different assumptions on the achieved systematic uncertainty, from weakest to strongest sensitivity: 0.6% correlated among detector modules at one site, 0.38% correlated, 0.38% uncorrelated among modules, 0.18% uncorrelated.

detectors. Various systematics are included with proper correlations between detectors and reactors, as well as backgrounds from accidental, fast neutrons, and cosmogenics according to the numbers provided in the respective proposals. Reactor fluxes and their uncertainties are included following [176].

The θ_{13} sensitivity limit time evolution is shown in fig. 18. We observe that the global sensitivity limit will be dominated by reactor experiments. If the assumed schedules for the reactor experiments are achieved, Double Chooz and RENO will each dominate the limit between 0.5 and one year, whereas as soon as operational Daya Bay will set the global limit. Thanks to the large exposure, Daya Bay will have the best limit (as well as discovery potential) among the reactor experiments. After 5 years of running the limits at 90% CL will be $\sin^2 2\theta_{13} = 0.026$ and 0.019 for Double Chooz and RENO, respectively, whereas the Daya Bay limit will range from 0.012 to 0.006 , depending on the systematics. In fig. 18 we show the Daya Bay limit under various assumptions about the relative normalisation uncertainty of their detectors, as discussed in section 5.2. Even for the most pessimistic assumption, Daya Bay will set the final limit on θ_{13} in the case no finite value will be discovered.

In case of no signal, the θ_{13} limit from beam experiments suffers from the marginalization over the CP phase and the mass hierarchy, as discussed in section 5.1. This situation is very different in case of the discovery potential, since there a favourable value of δ can greatly enhance the sensitivity of the appearance experiments. The θ_{13} discovery potentials are shown in fig. 19 as a function of time. For the beam experiments, the dependence on the true value of δ is reflected by the interval between the solid curves

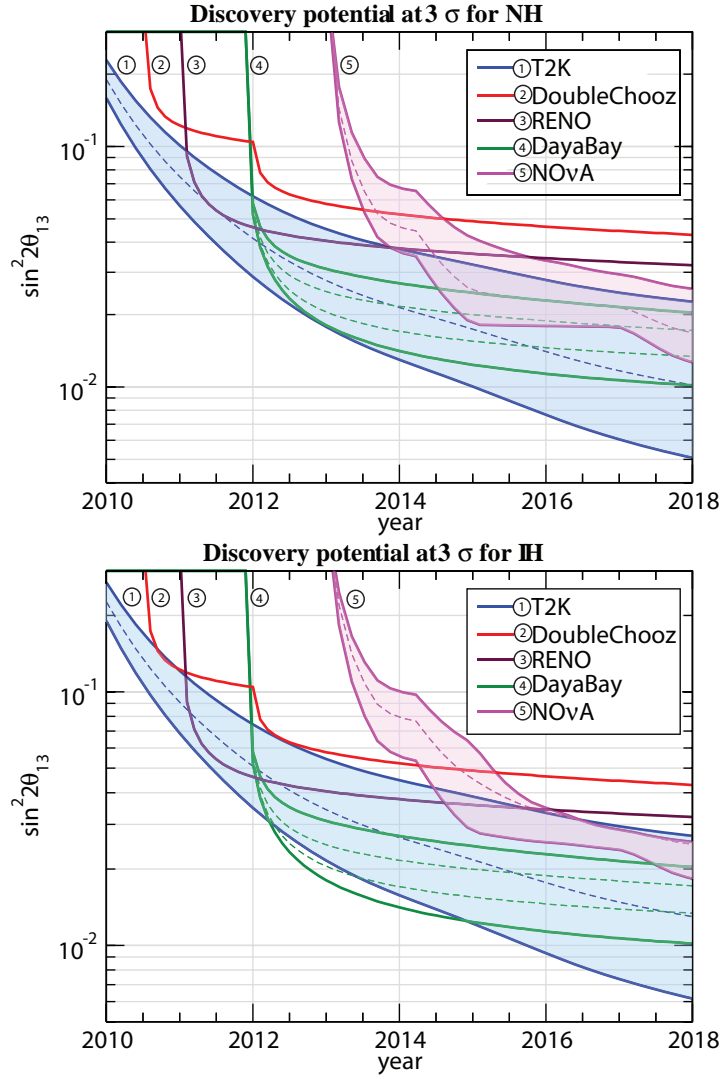


Figure 19. Evolution of the θ_{13} discovery potential as a function of time (3σ CL), i.e., the smallest value of θ_{13} which can be distinguished from zero at 3σ . We assume the normal and inverted simulated hierarchies in the top and bottom panels, respectively. The bands for the beams reflect the (unknown) true value of δ . For the dashed curves $\delta = 0$ has been fixed. The four curves for Daya Bay correspond to different assumptions on the achieved systematic uncertainty, from weakest to strongest sensitivity: 0.6% correlated among detector modules at one site, 0.38% correlated, 0.38% uncorrelated among modules, 0.18% uncorrelated.

for a given time (shaded regions). The dashed curves for T2K and NO ν A correspond to a fixed value for the CP phase of $\delta = 0$. ¶ The reactor experiments are not affected by the true δ ; the various curves for Daya Bay again correspond to the different assumptions concerning systematics as described above. There is a small dependence on the true mass hierarchy for the beam experiments, compare top and bottom panels, where for IH the sensitivity is slightly worse because of the suppression of the oscillation probability for

¶ Evolution of sensitivities under this condition have been shown recently in [177, 178].

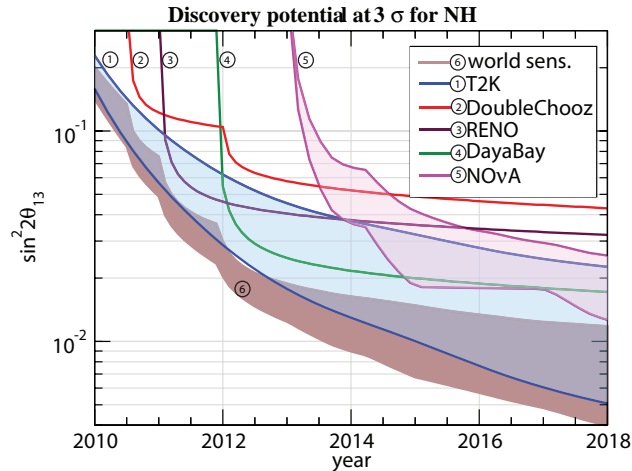


Figure 20. Evolution of the θ_{13} discovery potential as a function of time (3σ CL) for NH, showing the global sensitivity reach. The bands for the beams and the global reach reflect the (unknown) true value of δ . For Daya Bay we have assumed a systematical uncertainty of 0.38% correlated among detector modules at one site.

neutrinos by the matter effect.

The comparison of Figs. 19 and 18 shows that suitable values of δ may significantly improve the discovery potential of beams compared to their sensitivity limit. Indeed, T2K may discover θ_{13} for smaller θ_{13} than Daya Bay in a significant fraction of the parameter space, depending on the achieved systematics in Daya Bay. The NO ν A band becomes more narrow due to the complementary information from the anti-neutrino running, with the clear disadvantage of being somewhat late.

In figure 20 we illustrate how the world sensitivity to θ_{13} could look like under the assumptions of the above schedules and that at each point in time a combined analysis of all available data is performed. The discovery reach will be set roughly by the optimal sensitivity of T2K, where the reactor experiments play an important role in providing sensitivity for the values of δ unfavourable for T2K. This plot nicely illustrates the interplay between reactor and beam experiments and shows that the global reach can be enhanced significantly if experiments of both types are available simultaneously with comparable sensitivities.

Let us comment also on the dependence of the sensitivities on the assumption $\sin^2 \theta_{23} = 0.5$. This is relevant only for beam experiments, since the survival probability in the reactor experiments is independent of θ_{23} , see eq. 29. In the range $0.4 < \sin^2 \theta_{23} < 0.6$ (corresponding roughly to the current 2σ allowed range [14]) the effect for the beam experiments is small [167]. The sensitivity to θ_{13} becomes somewhat better the larger $\sin^2 \theta_{23}$, which follows from the first term in eq. 30. In these cases the choice $\sin^2 \theta_{23} = 0.5$ corresponds to the “average” situation.

Note that this discussion is based on the unitary standard three-flavour oscillation framework. If the search for new physics is taken into account, different reactor experiments, or reactor experiments and superbeams, may imply different information

and therefore be very complementary; see, e.g., Refs. [179, 180].

5.4. On the interpretation of sensitivities for future experiments

A widely used procedure to calculate sensitivities for future experiments is to assume some input values (“true” or “simulated” values) for the oscillation parameters for which the predictions for the observables in a given experiment are calculated without statistical fluctuations. Then these predictions are used as “data” and a statistical analysis of these data is performed to see how well the input values for the parameters can be reconstructed by the experiment. This procedure, denoted by “standard” procedure in the following, should give the sensitivity of an “average” experiment, where “average” lacks a precise definition. The results of the previous subsections are obtained by this method, and most of the sensitivity studies for future neutrino oscillation experiments in the literature are based on this procedure. In particular the GLoBES long-baseline experiment simulation software [133, 134] is designed for this method.

Ref. [181] clarifies the correct interpretation of such sensitivities in the context of oscillation experiments. Monte Carlo simulations of the Double Chooz and T2K experiments are performed in order to address the following question in a frequentist framework: *Given a true value of θ_{13} , what is the probability that the hypothesis $\theta_{13} = 0$ can be excluded at a certain confidence level?* This generalises the usual sensitivity limits to a well defined statistical statement and allows also a precise definition of the “average experiment”. For example one may define the sensitivity of an average experiment as the value of $\theta_{13}^{\text{true}}$ for which $\theta_{13} = 0$ can be excluded with a probability of 50%.

A large number of artificial data sets is generated to calculate the actual distribution of the statistics used to decide whether $\theta_{13} = 0$ should be rejected at a given confidence level. This allows to answer the question stated above within a well defined frequentist framework. Moreover one does not rely on questionable assumptions necessary in the standard procedure, for example issues related to the non-linear character of the parameters, the periodicity of the CP phase δ , the physical boundary $\sin^2 2\theta_{13} \geq 0$, assuming standard χ^2 -distributions, and the question of how many degrees of freedom to use for them. Note that the specific experimental configurations and parameters used for the simulations in [181] for Double Chooz and T2K differ slightly from the most up-to-date versions.

The probability $P_{\text{disc}}(\alpha, \theta_{13})$ that $\theta_{13} = 0$ can be excluded at the $100(1 - \alpha)\%$ CL is given by

$$P_{\text{disc}}(\alpha, \theta_{13}) \equiv P [\Delta\chi_0^2 > \lambda(\alpha) \mid \theta_{13}] = \int_{\lambda(\alpha)}^{\infty} dx f_{\theta_{13}}(x). \quad (31)$$

Here $\Delta\chi_0^2 \equiv \chi^2(\theta_{13} = 0) - \chi_{\text{min}}^2$ is the difference in χ^2 between the best fit point and $\theta_{13} = 0$, $\lambda(\alpha)$ is the $\Delta\chi^2$ value corresponding to the $100(1 - \alpha)\%$ confidence level, and $f_{\theta_{13}}(\Delta\chi_0^2)$ is the distribution of $\Delta\chi_0^2$ for a fixed true value of θ_{13} . The distribution $f_{\theta_{13}}(\Delta\chi_0^2)$ and the values of $\lambda(\alpha)$ have been obtained by Monte Carlo simulation.

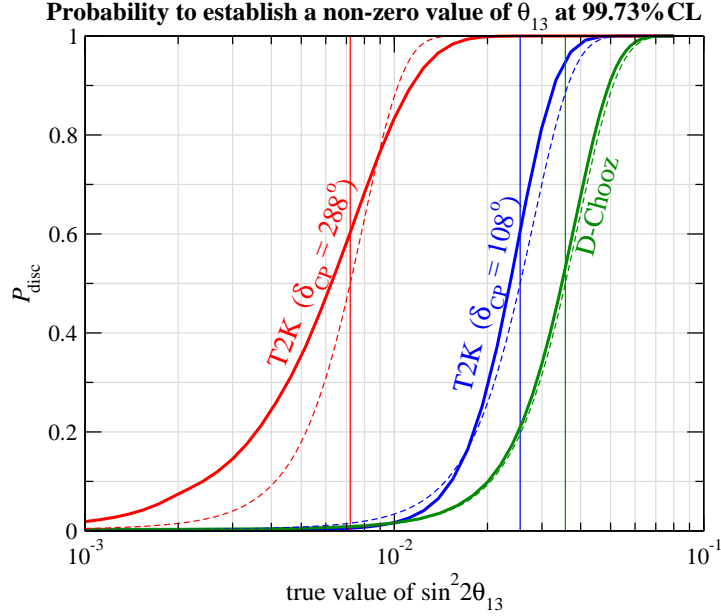


Figure 21. The probability to exclude the hypothesis $\theta_{13} = 0$ at the 99.73% CL for T2K and Double Chooz as a function of the true value of $\sin^2 2\theta_{13}$. The two curves for T2K correspond to the true values $\delta = 108^\circ$ and 288° . The vertical lines show the corresponding “standard” sensitivities. The dashed curves correspond to the probability P_{disc} calculated in the Gaussian approximation according to eq. 32. Reprinted from Ref. [181], Copyright (2007), with permission from Elsevier.

Fig. 21 shows the probability P_{disc} to exclude the hypothesis $\theta_{13} = 0$ at the 99.73% CL for T2K and Double Chooz as a function of the true value of $\sin^2 2\theta_{13}$. For each true value 3×10^6 data sets have been simulated. For T2K the two values chosen for δ correspond roughly to the best and worst sensitivity. The vertical lines in the plot show the standard sensitivities calculated from the condition $\Delta\chi^2 \geq 9$ without statistical fluctuations. One observes that for Double Chooz the standard sensitivity corresponds indeed with good accuracy to $P_{\text{disc}} = 50\%$, as expected for an “average” experiment. For T2K the discovery probabilities corresponding to the standard sensitivities are actually slightly higher, around 60%.

The dashed curves shown in fig. 21 are obtained assuming a Gaussian measurement of $\sin^2 2\theta_{13}$. In this case P_{disc} can be obtained in terms of the error function in the following way. Assuming that x is a Gaussian variable with standard deviation σ the hypothesis $x = 0$ can be excluded at the 99.73% CL if the observed value x^{obs} is bigger than 3σ . On the other hand, the probability for $x^{\text{obs}} \geq 3\sigma$ as a function of the true value x^{true} is easily calculated as

$$P[x^{\text{obs}} \geq 3\sigma | x^{\text{true}}] = \int_{3\sigma}^{\infty} dx G(x; x^{\text{true}}, \sigma) = \frac{1}{2} \left[1 - \text{erf} \left(\frac{3\sigma - x^{\text{true}}}{\sqrt{2}\sigma} \right) \right], \quad (32)$$

where $G(x; x^{\text{true}}, \sigma)$ denotes the normal distribution with mean x^{true} and standard deviation σ .

The dashed curves in fig. 21 have been obtained from eq. 32 by identifying

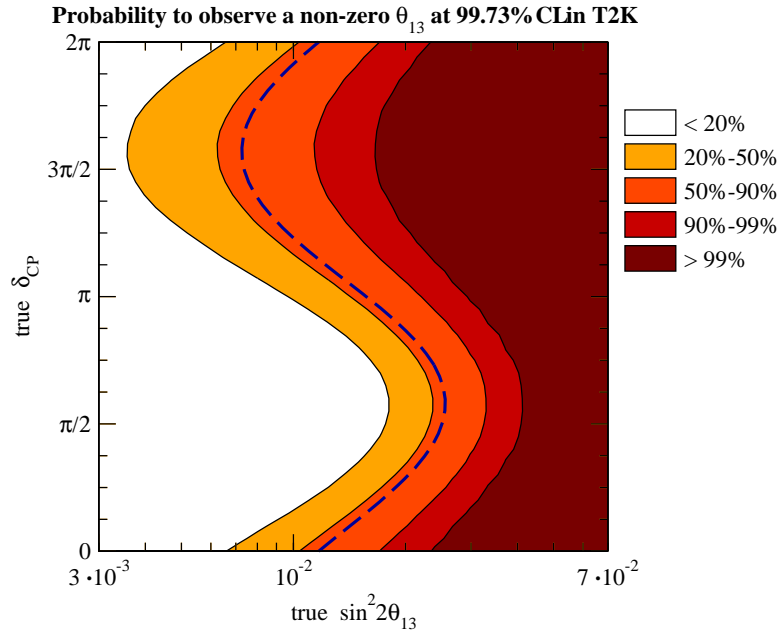


Figure 22. Contours of the probability P_{disc} to establish a non-zero value of θ_{31} at the 99.73% CL for T2K in the $\sin^2 2\theta_{13}^{\text{true}}-\delta^{\text{true}}$ plane. The dashed curve corresponds to the “standard sensitivity limit”. Reprinted from Ref. [181], Copyright (2007), with permission from Elsevier.

$\sin^2 2\theta_{13} = x$ and by using for σ one third of the 99.73% CL sensitivity limit from the standard procedure. One observes that for Double Chooz this approximation is excellent. Hence, in this case $\sin^2 2\theta_{13}$ can be considered indeed as a Gaussian variable and the probability P_{disc} can be calculated from the standard sensitivity limit and eq. 32 without the need of a MC simulation. In contrast, for T2K some deviations from Gaussianity are visible (especially for $\delta^{\text{true}} = 288^\circ$). This is not unexpected, since in this case event numbers are small, background fluctuations are important, and the dependence of the observables on the parameters is much more complicated than in the case of Double Chooz.

Contours of the probability P_{disc} for the T2K experiment in the plane of $\sin^2 2\theta_{13}^{\text{true}}$ and δ^{true} are shown in fig. 22. P_{disc} has been calculated for a grid of 41×41 values and at each point in the grid 10^5 data sets have been generated, leading in total to nearly 1.7×10^8 performed fits. This figure is the generalisation of the usual sensitivity limit (shown as dashed curve) and for each true value of the parameters one can infer the probability that T2K can establish a non-zero value of θ_{13} at the 99.73% CL. As indicated already in fig. 21 one finds that the standard sensitivity curve corresponds roughly to a discovery probability of 60%. The region where $\theta_{13} > 0$ can be established with high probability, let’s say greater than 99%, is found for $\sin^2 2\theta_{13}^{\text{true}} > 0.0166 - 0.041$, depending on the true value of δ . It is shifted with respect to the standard sensitivity limit to values of $\sin^2 2\theta_{13}$ larger by roughly a factor of 2.

In summary, for Double Chooz (and reactor experiments in general) the Gaussian approximation is very well justified. The usually calculated sensitivity corresponds to

the performance of an average experiment (the discovery will be made with a probability of 50%), and the actual discovery probability can be estimated by a simple formula in terms of the error function. In the case of appearance beam experiments some deviations from Gaussianity are found. For T2K the standard sensitivity limits correspond to a discovery probability of about 60%. The results of [181] confirm that standard sensitivity limits provide a reasonable approximation for an average experiment, corresponding to a discovery probability of order 50%. However, one has to be aware of the correct interpretation of such limits. In general the region where a discovery can be made with high probability is significantly smaller than the one corresponding to the standard sensitivity limits.

6. A subsequent generation of experiments

If the upcoming generation of experiments discussed in this review cannot establish a finite value of θ_{13} , experiments able to explore the region $\sin^2 2\theta_{13} < 10^{-2}$ will be needed. On the other hand, if a positive signal can be established this generation of experiments will not be sensitive enough to make a firm discovery (3σ or better) of leptonic CP violation and the neutrino mass hierarchy, see Fig. 14 and the extensive discussion in Ref. [167]. In this section we briefly outline some possibilities for such high precision oscillation facilities, more complete discussions can be found in [29, 33].

A possible way to attack the searches of leptonic CP violation is to push conventional neutrino beams to their ultimate performances and build huge detectors, one order of magnitude, at least, bigger than the present detectors. As an example T2K could be upgraded, as already delineated in the initial LoI [24], by pushing the power of the J-PARC Main Ring to 4 MW (2 MW seems nowadays more realistic) and building a water Čerenkov detector of about 500 kton fiducial volume, HyperKamiokande, more than 20 times bigger than SuperKamiokande, to be placed at the same distance and the same off-axis angle as SuperKamiokande. Subsequent developments of this project foresee the possibility of placing half of the detector at a longer distance, about 900 km in Korea, T2KK [182], or to substitute it with a 100 kton liquid argon detector placed at 658 km from J-PARC at a smaller off-axis angle of 0.5° [183]. The longer baselines would provide better sensitivities to the mass hierarchy and better control of degeneracies. In the United States a similar project designs a wide-band beam (WBB) [184] generated by the FNAL Main Injector and fired to a 300 kton water Čerenkov detector placed at the DUSEL lab, 1290 km far away from FNAL (3 ÷ 6 liquid argon modules of 20 kton are also taken in consideration).

In Europe, superbeams have been proposed based on upgrades of the CNGS beam [139, 140], or on a high power version of accelerators foreseen for a possible new injection chain of the LHC [185] as the SPL and the PS2. It appears very difficult [186] to set the performances of the CNGS beam to the level needed for searches of leptonic CP violation, that is 10 times the protons actually generated on target. The SPL superbeam [187], based on the 3.5 GeV, 4 MW Superconducting

Proton Linac [188], can generate a neutrino beam of about 300 MeV sent to a 500 kton water Čerenkov detector (MEMPHYS [189]) placed in Fréjus at 130 km from CERN. It would have excellent sensitivities for θ_{13} and leptonic CP violation [125], while the mass hierarchy sensitivity would be limited by the relatively short baseline (the synergy with atmospheric neutrinos [73] would provide sensitivity to the mass hierarchy at large values of θ_{13} [125]).

It has been proposed in [190] to generate a neutrino beam by a high power (1.6 MW) version of the PS2 accelerator, a 50 GeV synchrotron designed to run at 0.4 MW to serve as a component of the new injection scheme for the LHC. Neutrinos could be then fired to a 100 kton liquid argon detector, placed at distances between 950 km or 1544 km or 2300 km. The distances correspond to the three underground labs of Sieroszowice in Poland, Slanic in Romania and Pyhasalmi in Finland, respectively, considered by the LAGUNA FP7 Design Study [191]. As in the case of the WBB at DUSEL, this setup would measure neutrinos at the first and at the second oscillation maximum. Liquid argon is certainly the best candidate to fulfill the requirements of this configuration. This kind of configuration would have excellent performances in measuring the sign of Δm_{31}^2 but a limited sensitivity for leptonic CP violation and the measurement of θ_{13} .

Sensitivities on θ_{13} of these future superbeams could reach the $\sin^2(2\theta_{13}) \simeq 10^{-3}$ level, as illustrated in Fig. 23. Similarly also leptonic CP violation could be performed in the same range of θ_{13} values, see e.g., [29, 30, 33].

The main limitations of conventional neutrino beams are the intrinsic ν_e contamination of the beam produced by the decay-in-flight of the kaons produced at the target and by the muons from the pion decays, and the uncertainty of the beam flux prediction due to the finite precision with which the hadron production cross sections can be known. The intrinsic limitations of conventional neutrino beams can be overcome if the neutrino parents are fully selected, collimated and accelerated to a given energy. This can be attempted within the muon lifetime (neutrino factory [25]) or within beta decaying ion lifetimes (beta beam [26]). In this way very pure, intense and precisely known neutrino beams can be designed.

The beta beam [26] is a facility based on the decay in flight of β -unstable ions, for reviews see [27, 28]. They are ideal tools to study $\nu_e \rightarrow \nu_\mu$ transitions and their CP-conjugate without any intrinsic source of backgrounds. The original proposal of Ref. [26] was tuned to leverage at most the present facilities of CERN (the PS and the SPS) and it was based on ${}^6\text{He}$ and ${}^{18}\text{Ne}$ as $\bar{\nu}_e$ and ν_e sources, respectively. These ions are accelerated to $\gamma = 100$ [195] and stored in a decay ring of about 7 km. With MEMPHYS as a far detector at Fréjus, this set-up could outperform any superbeam configuration in terms of sensitivity to θ_{13} and leptonic CP violation [125], and these performances would be significantly enhanced if the SPL superbeam would be fired to the same far detector [125, 196]. Accelerating the same ions to $\gamma = 350$ (an option that requires a 1 TeV accelerator) the performances of the beta beam would be significantly improved [197, 198]. Various even more ambitious beta beam configurations are discussed in the literature, including very high γ factors as well as exploring different isotopes,

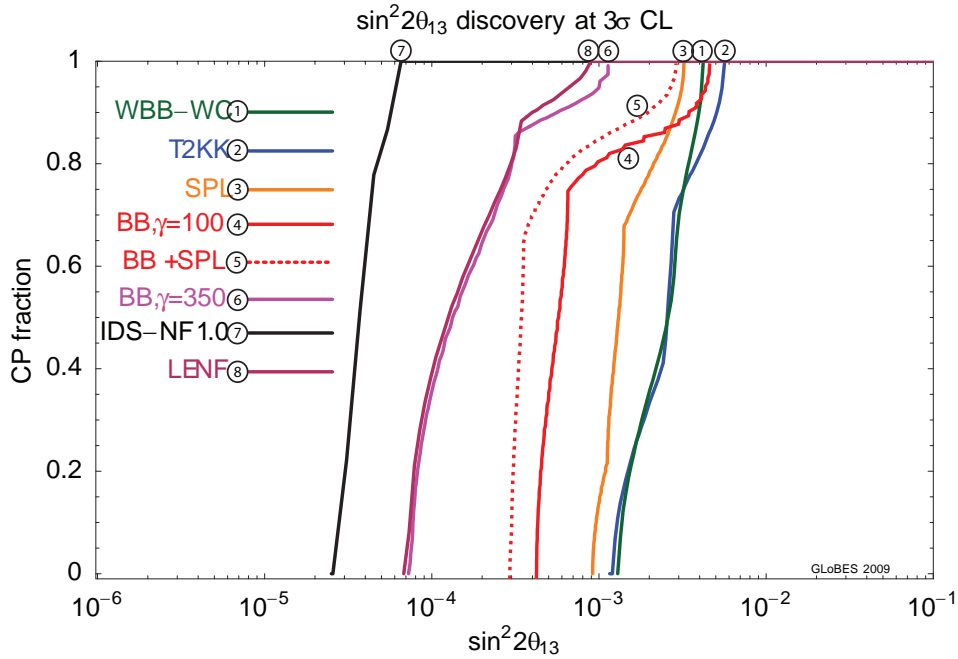


Figure 23. 3σ discovery sensitivity to $\sin^2 2\theta_{13}$ as a function of the fraction of all possible values of δ_{CP} , computed for 10 years of data taking and 5% systematic errors (2% for the neutrino factory). The curve labelled WBB-WC refers to the FNAL-DUSEL setup [192], the curves for the SPL superbeam, the $\gamma = 100$ beta beam and their combination are taken from [125], the curve for the $\gamma = 350$ beta beam is taken from [193], the low energy neutrino factory (LENF) from [194], and IDS-NF corresponds to a hypothetical neutrino factory scenario with two 100 kton magnetized iron detectors at 4000 and 7500 km and an Emulsion Cloud Chamber detector to detect $\nu_e \rightarrow \nu_\tau$ transitions at 4000 km taken from [33]. The plot has been adapted from a figure prepared by P. Huber for the EURO ν WP6 study [33].

see [33] for a recent summary and references.

Production, acceleration and stacking of high intensity muon beams for muon colliders have been envisaged thanks to their decays producing useful beams of ν_μ and $\bar{\nu}_e$ (exploiting μ^- decays into $e^- \bar{\nu}_e \nu_\mu$) or $\bar{\nu}_\mu$ and ν_e (μ^+ decays into $e^+ \nu_e \bar{\nu}_\mu$). In a “Neutrino Factory” [25], muons are created from an intense pion source at low energies, their phase space is compressed to produce a bright muon beam, which is then accelerated to the desired energy and injected into a storage ring with long straight sections pointing in the desired direction. The neutrino factory design can be considered as strongly physics-motivated intermediate step towards a muon collider [199].

Assuming μ^+ in the decay ring, one looks for $\nu_e \rightarrow \nu_\mu$ oscillations due to the appearance of μ^- from ν_μ CC events in the detector (“wrong sign muons”), which have to be separated from the bulk of μ^+ (“right sign muons”) coming from unoscillated $\bar{\nu}_\mu$. A suitable detector to search for these transitions is a magnetized iron detector [200, 201]. As pointed out in [202], a neutrino factory would be an ideal tool to address CP violation in the leptonic sector, with outstanding performances compared with pion-based sources. The realization of the neutrino factory still represents a major accelerator challenge

compared with neutrino superbeams.

We report in Fig. 23 a comparison of θ_{13} sensitivities of some examples for the facilities described in this section.

7. Conclusions

In this review we have summarized the present status of the last unknown lepton mixing angle θ_{13} and discussed the experimental progress to be expected within the next years. Although there are some hints for a non-zero value of θ_{13} in current neutrino oscillation data, at present we can only quote an upper bound of $\sin^2 \theta_{13} < 0.031$ at 90% CL from global data. Best fit points obtained by different groups range from $\sin^2 \theta_{13} \simeq 0.01$ to 0.02, being consistent with $\theta_{13} = 0$ at the 1 to 2σ level, see Tab. 1 for a summary.

Several new neutrino oscillation experiments will contribute significantly to our information on θ_{13} in the near future. The reactor experiments Daya Bay, Double Chooz, and RENO as well as the accelerator experiments NO ν A and T2K have been presented in section 4. The time evolution for the sensitivity to θ_{13} from these experiments is summarised in the figures 18 and 19. Within the next few years values of $\sin^2 2\theta_{13}$ down to 10^{-2} will be probed, about one order of magnitude smaller than the current upper bound. These results will be of fundamental importance for the better understanding of the lepton sector, the problem of flavour and in particular for the question whether the values of the lepton mixing matrix indicate the presence of a flavour symmetry. The results of those experiments will be a corner stone for any subsequent neutrino oscillation facility aiming at the ultimate goals like the discovery of CP violation in the lepton sector or the determination of the neutrino mass hierarchy.

Acknowledgements

We thank Mark Messier for information on the NO ν A experiment, Soo-Bong Kim for information on the RENO experiment and Kam-Biu Luk for information on the Daya Bay experiment. We acknowledge the financial support of the European Community under the European Commission Framework Programme 7 Design Studies: EUROnu, Project Number 212372 and LAGUNA, Project Number 212343. The EC is not liable for any use that may be made of the information contained herein. The work of TS is partly supported by the Transregio Sonderforschungsbereich TR27 “Neutrinos and Beyond” der Deutschen Forschungsgemeinschaft.

References

- [1] B. T. Cleveland *et al.*, *Measurement of the solar electron neutrino flux with the Homestake chlorine detector*, *Astrophys. J.* **496**, 505 (1998).
- [2] GNO, M. Altmann *et al.*, *Complete results for five years of GNO solar neutrino observations*, *Phys. Lett.* **B616**, 174 (2005), hep-ex/0504037.

- [3] Super-Kamiokande, J. Hosaka *et al.*, *Solar neutrino measurements in Super-Kamiokande-I*, Phys. Rev. **D73**, 112001 (2006), hep-ex/0508053.
- [4] SNO, Q. R. Ahmad *et al.*, *Direct evidence for neutrino flavor transformation from neutral-current interactions in the Sudbury Neutrino Observatory*, Phys. Rev. Lett. **89**, 011301 (2002), nucl-ex/0204008.
- [5] SNO, B. Aharmim *et al.*, *An Independent Measurement of the Total Active 8B Solar Neutrino Flux Using an Array of 3He Proportional Counters at the Sudbury Neutrino Observatory*, Phys. Rev. Lett. **101**, 111301 (2008), 0806.0989.
- [6] SNO, B. Aharmim *et al.*, *Low Energy Threshold Analysis of the Phase I and Phase II Data Sets of the Sudbury Neutrino Observatory*, (2009), 0910.2984.
- [7] Borexino, C. Arpesella *et al.*, *Direct Measurement of the Be-7 Solar Neutrino Flux with 192 Days of Borexino Data*, Phys. Rev. Lett. **101**, 091302 (2008), 0805.3843.
- [8] Super-Kamiokande, Y. Fukuda *et al.*, *Evidence for oscillation of atmospheric neutrinos*, Phys. Rev. Lett. **81**, 1562 (1998), hep-ex/9807003.
- [9] Super-Kamiokande, Y. Ashie *et al.*, *A measurement of atmospheric neutrino oscillation parameters by Super-Kamiokande I*, Phys. Rev. **D71**, 112005 (2005), hep-ex/0501064.
- [10] KamLAND, T. Araki *et al.*, *Measurement of neutrino oscillation with KamLAND: Evidence of spectral distortion*, Phys. Rev. Lett. **94**, 081801 (2005), hep-ex/0406035.
- [11] KamLAND, S. Abe *et al.*, *Precision Measurement of Neutrino Oscillation Parameters with KamLAND*, Phys. Rev. Lett. **100**, 221803 (2008), 0801.4589.
- [12] K2K, M. H. Ahn *et al.*, *Measurement of neutrino oscillation by the K2K experiment*, Phys. Rev. **D74**, 072003 (2006), hep-ex/0606032.
- [13] MINOS, P. Adamson *et al.*, *Measurement of Neutrino Oscillations with the MINOS Detectors in the NuMI Beam*, Phys. Rev. Lett. **101**, 131802 (2008), 0806.2237.
- [14] T. Schwetz, M. A. Tortola, and J. W. F. Valle, *Three-flavour neutrino oscillation update*, New J. Phys. **10**, 113011 (2008), 0808.2016.
- [15] CHOOZ, M. Apollonio *et al.*, *Search for neutrino oscillations on a long base-line at the CHOOZ nuclear power station*, Eur. Phys. J. **C27**, 331 (2003), hep-ex/0301017.
- [16] F. Boehm *et al.*, *Final results from the Palo Verde neutrino oscillation experiment*, Phys. Rev. **D64**, 112001 (2001), hep-ex/0107009.
- [17] G. L. Fogli, E. Lisi, A. Marrone, A. Palazzo, and A. M. Rotunno, *Hints of $\theta_{13} > 0$ from global neutrino data analysis*, Phys. Rev. Lett. **101**, 141801 (2008), 0806.2649.
- [18] M. C. Gonzalez-Garcia, M. Maltoni, and J. Salvado, *Updated global fit to three neutrino mixing: status of the hints of $\theta_{13} > 0$* , (2010), 1001.4524.
- [19] MINOS, P. Adamson *et al.*, *Search for muon-neutrino to electron-neutrino transitions in MINOS*, Phys. Rev. Lett. **103**, 261802 (2009), 0909.4996.
- [20] Daya-Bay, X. Guo *et al.*, *A precision measurement of the neutrino mixing angle θ_{13} using reactor antineutrinos at Daya Bay*, (2007), hep-ex/0701029.
- [21] Double Chooz, F. Ardellier *et al.*, *Double Chooz: A search for the neutrino mixing angle θ_{13}* , (2006), hep-ex/0606025.
- [22] RENO, J. K. Ahn *et al.*, *RENO: An Experiment for Neutrino Oscillation Parameter θ_{13} Using Reactor Neutrinos at Yonggwang*, (2010), 1003.1391.
- [23] NOvA, I. Ambats *et al.*, *NOvA proposal to build a 30-kiloton off-axis detector to study neutrino oscillations in the Fermilab NuMI beamline*, (2004), hep-ex/0503053.
- [24] Y. Itow *et al.*, *The JHF-Kamioka neutrino project*, Nucl. Phys. Proc. Suppl. **111**, 146 (2001), hep-ex/0106019.
- [25] S. Geer, *Neutrino beams from muon storage rings: Characteristics and physics potential*, Phys. Rev. **D57**, 6989 (1998), hep-ph/9712290.
- [26] P. Zucchelli, *A novel concept for a $\bar{\nu}_e / \nu_e$ neutrino factory: The beta beam*, Phys. Lett. **B532**, 166 (2002).
- [27] C. Volpe, *Topical review on 'beta-beams'*, J. Phys. **G34**, R1 (2007), hep-ph/0605033.

- [28] M. Lindroos and M. Mezzetto, *Beta beams: Neutrino beams*, London, UK: Imperial College Pr. (2010) 154 p.
- [29] ISS Physics Working Group, A. Bandyopadhyay *et al.*, *Physics at a future Neutrino Factory and super-beam facility*, Rept. Prog. Phys. **72**, 106201 (2009), 0710.4947.
- [30] V. Barger *et al.*, *Report of the US long baseline neutrino experiment study*, (2007), 0705.4396.
- [31] European Commission FP7 Design Study: A High Intensity Neutrino Oscillation Facility in Europe, <http://www.euronu.org>.
- [32] International design study of the neutrino factory, <http://www.ids-nf.org>.
- [33] J. Bernabeu *et al.*, *EUROν WP6 2009 yearly report: Update of the physics potential of Nufact, superbeams and betabeams*, (2010), 1005.3146.
- [34] Y. Giomataris and J. D. Vergados, *Neutrino properties studied with a triton source using large TPC detectors*, Nucl. Instrum. Meth. **A530**, 330 (2004), hep-ex/0303045.
- [35] S. Aune *et al.*, *NOSTOS: A spherical TPC to detect low energy neutrinos*, AIP Conf. Proc. **785**, 110 (2005), hep-ex/0503031.
- [36] R. S. Raghavan, *Recoilless resonant capture of antineutrinos*, (2005), hep-ph/0511191.
- [37] H. Minakata and S. Uchinami, *Recoilless resonant absorption of monochromatic neutrino beam for measuring Δm_{31}^2 and θ_{13}* , New J. Phys. **8**, 143 (2006), hep-ph/0602046.
- [38] W. Potzel, *Moessbauer antineutrinos: some basic considerations*, Acta Phys. Polon. **B40**, 3033 (2009), 0912.2221.
- [39] J. Kopp, *Mossbauer neutrinos in quantum mechanics and quantum field theory*, JHEP **06**, 049 (2009), 0904.4346.
- [40] E. K. Akhmedov, J. Kopp, and M. Lindner, *Oscillations of Mossbauer neutrinos*, JHEP **05**, 005 (2008), 0802.2513.
- [41] C. Lunardini and A. Y. Smirnov, *Probing the neutrino mass hierarchy and the 13-mixing with supernovae*, JCAP **0306**, 009 (2003), hep-ph/0302033.
- [42] J. Gava, J. Kneller, C. Volpe, and G. C. McLaughlin, *A dynamical collective calculation of supernova neutrino signals*, Phys. Rev. Lett. **103**, 071101 (2009), 0902.0317.
- [43] B. Dasgupta, G. G. Raffelt, and I. Tamborra, *Triggering collective oscillations by three-flavor effects*, (2010), 1001.5396.
- [44] Y. Farzan and A. Y. Smirnov, *Leptonic unitarity triangle and CP-violation*, Phys. Rev. **D65**, 113001 (2002), hep-ph/0201105.
- [45] M. Lindner, A. Merle, and W. Rodejohann, *Improved limit on θ_{13} and implications for neutrino masses in neutrino-less double beta decay and cosmology*, Phys. Rev. **D73**, 053005 (2006), hep-ph/0512143.
- [46] C. Giunti and M. Laveder, *VSBL Electron Neutrino Disappearance*, Phys. Rev. **D80**, 013005 (2009), 0902.1992.
- [47] P. D. Serpico and M. Kachelriess, *Measuring the 13-mixing angle and the CP phase with neutrino telescopes*, Phys. Rev. Lett. **94**, 211102 (2005), hep-ph/0502088.
- [48] W. Winter, *How astrophysical neutrino sources could be used for early measurements of neutrino mass hierarchy and leptonic CP phase*, Phys. Rev. **D74**, 033015 (2006), hep-ph/0604191.
- [49] M. Blennow, J. Edsjo, and T. Ohlsson, *Neutrinos from WIMP Annihilations Using a Full Three-Flavor Monte Carlo*, JCAP **0801**, 021 (2008), 0709.3898.
- [50] R. Lehnert and T. J. Weiler, *Flavor sensitivity to θ_{13} and the mass hierarchy for neutrinos from solar WIMP annihilation*, (2010), 1002.2441.
- [51] M. Maltoni and T. Schwetz, *Sterile neutrino oscillations after first MiniBooNE results*, Phys. Rev. **D76**, 093005 (2007), 0705.0107.
- [52] G. Karagiorgi, Z. Djurcic, J. M. Conrad, M. H. Shaevitz, and M. Sorel, *Viability of $\Delta m^2 \sim 1$ eV² sterile neutrino mixing models in light of MiniBooNE electron neutrino and antineutrino data from the Booster and NuMI beamlines*, Phys. Rev. **D80**, 073001 (2009), 0906.1997.
- [53] C. Biggio, M. Blennow, and E. Fernandez-Martinez, *General bounds on non-standard neutrino interactions*, JHEP **08**, 090 (2009), 0907.0097.

- [54] S. Antusch, J. P. Baumann, and E. Fernandez-Martinez, *Non-Standard Neutrino Interactions with Matter from Physics Beyond the Standard Model*, Nucl. Phys. **B810**, 369 (2009), 0807.1003.
- [55] M. B. Gavela, D. Hernandez, T. Ota, and W. Winter, *Large gauge invariant non-standard neutrino interactions*, Phys. Rev. **D79**, 013007 (2009), 0809.3451.
- [56] Z. Maki, M. Nakagawa, and S. Sakata, *Remarks on the unified model of elementary particles*, Prog. Theor. Phys. **28**, 870 (1962).
- [57] B. Pontecorvo, *Neutrino experiments and the question of leptonic-charge conservation*, Sov. Phys. JETP **26**, 984 (1968).
- [58] J. Gluza and M. Zralek, *Parameters' domain in three flavour neutrino oscillations*, Phys. Lett. **B517**, 158 (2001), hep-ph/0106283.
- [59] L. Wolfenstein, *Neutrino oscillations in matter*, Phys. Rev. **D17**, 2369 (1978).
- [60] V. D. Barger, K. Whisnant, S. Pakvasa, and R. J. N. Phillips, *Matter effects on three-neutrino oscillations*, Phys. Rev. **D22**, 2718 (1980).
- [61] S. P. Mikheev and A. Y. Smirnov, *Resonance enhancement of oscillations in matter and solar neutrino spectroscopy*, Sov. J. Nucl. Phys. **42**, 913 (1985).
- [62] S. P. Mikheev and A. Y. Smirnov, *Resonant amplification of neutrino oscillations in matter and solar neutrino spectroscopy*, Nuovo Cim. **C9**, 17 (1986).
- [63] M. Fukugita and T. Yanagida, *Baryogenesis Without Grand Unification*, Phys. Lett. **B174**, 45 (1986).
- [64] N. Cabibbo, *Time Reversal Violation in Neutrino Oscillation*, Phys. Lett. **B72**, 333 (1978).
- [65] S. M. Bilenky, J. Hosek, and S. T. Petcov, *On Oscillations of Neutrinos with Dirac and Majorana Masses*, Phys. Lett. **B94**, 495 (1980).
- [66] V. D. Barger, K. Whisnant, and R. J. N. Phillips, *CP Violation in Three Neutrino Oscillations*, Phys. Rev. Lett. **45**, 2084 (1980).
- [67] C. Jarlskog, *Commutator of the Quark Mass Matrices in the Standard Electroweak Model and a Measure of Maximal CP Violation*, Phys. Rev. Lett. **55**, 1039 (1985).
- [68] H. Nunokawa, S. J. Parke, and J. W. F. Valle, *CP Violation and Neutrino Oscillations*, Prog. Part. Nucl. Phys. **60**, 338 (2008), 0710.0554.
- [69] M. Freund, M. Lindner, S. T. Petcov, and A. Romanino, *Testing matter effects in very long baseline neutrino oscillation experiments*, Nucl. Phys. **B578**, 27 (2000), hep-ph/9912457.
- [70] V. D. Barger, S. Geer, R. Raja, and K. Whisnant, *Determination of the pattern of neutrino masses at a neutrino factory*, Phys. Lett. **B485**, 379 (2000), hep-ph/0004208.
- [71] J. Bernabeu, S. Palomares Ruiz, and S. T. Petcov, *Atmospheric neutrino oscillations, θ_{13} and neutrino mass hierarchy*, Nucl. Phys. **B669**, 255 (2003), hep-ph/0305152.
- [72] D. Indumathi and M. V. N. Murthy, *A question of hierarchy: Matter effects with atmospheric neutrinos and anti-neutrinos*, Phys. Rev. **D71**, 013001 (2005), hep-ph/0407336.
- [73] P. Huber, M. Maltoni, and T. Schwetz, *Resolving parameter degeneracies in long-baseline experiments by atmospheric neutrino data*, Phys. Rev. **D71**, 053006 (2005), hep-ph/0501037.
- [74] S. T. Petcov and T. Schwetz, *Determining the neutrino mass hierarchy with atmospheric neutrinos*, Nucl. Phys. **B740**, 1 (2006), hep-ph/0511277.
- [75] S. T. Petcov and M. Piai, *The LMA MSW solution of the solar neutrino problem, inverted neutrino mass hierarchy and reactor neutrino experiments*, Phys. Lett. **B533**, 94 (2002), hep-ph/0112074.
- [76] H. Nunokawa, S. J. Parke, and R. Zukanovich Funchal, *Another possible way to determine the neutrino mass hierarchy*, Phys. Rev. **D72**, 013009 (2005), hep-ph/0503283.
- [77] A. de Gouvea, J. Jenkins, and B. Kayser, *Neutrino mass hierarchy, vacuum oscillations, and vanishing U_{e3}* , Phys. Rev. **D71**, 113009 (2005), hep-ph/0503079.
- [78] A. de Gouvea and W. Winter, *What would it take to determine the neutrino mass hierarchy if θ_{13} were too small?*, Phys. Rev. **D73**, 033003 (2006), hep-ph/0509359.
- [79] R. Gandhi, P. Ghoshal, S. Goswami, and S. U. Sankar, *Neutrino mass hierarchy determination*

- for $\theta_{13} = 0$, (2009), 0905.2382.
- [80] S. Pascoli, S. T. Petcov, and T. Schwetz, *The Absolute Neutrino Mass Scale, Neutrino Mass Spectrum, Majorana CP-Violation and Neutrinoless Double-Beta Decay*, Nucl. Phys. **B734**, 24 (2006), hep-ph/0505226.
 - [81] S. Choubey and W. Rodejohann, *Neutrinoless double beta decay and future neutrino oscillation precision experiments*, Phys. Rev. **D72**, 033016 (2005), hep-ph/0506102.
 - [82] A. S. Dighe, M. T. Keil, and G. G. Raffelt, *Detecting the neutrino mass hierarchy with a supernova at IceCube*, JCAP **0306**, 005 (2003), hep-ph/0303210.
 - [83] H. Duan, G. M. Fuller, J. Carlson, and Y.-Q. Zhong, *Neutrino Mass Hierarchy and Stepwise Spectral Swapping of Supernova Neutrino Flavors*, Phys. Rev. Lett. **99**, 241802 (2007), 0707.0290.
 - [84] B. Dasgupta, A. Dighe, and A. Mirizzi, *Identifying neutrino mass hierarchy at extremely small θ_{13} through Earth matter effects in a supernova signal*, Phys. Rev. Lett. **101**, 171801 (2008), 0802.1481.
 - [85] B. Dasgupta, A. Mirizzi, I. Tamborra, and R. Tomas, *Neutrino mass hierarchy and three-flavor spectral splits of supernova neutrinos*, (2010), 1002.2943.
 - [86] A. de Gouvea and H. Murayama, *Statistical test of anarchy*, Phys. Lett. **B573**, 94 (2003), hep-ph/0301050.
 - [87] P. F. Harrison, D. H. Perkins, and W. G. Scott, *Tri-bimaximal mixing and the neutrino oscillation data*, Phys. Lett. **B530**, 167 (2002), hep-ph/0202074.
 - [88] V. D. Barger, S. Pakvasa, T. J. Weiler, and K. Whisnant, *Bi-maximal mixing of three neutrinos*, Phys. Lett. **B437**, 107 (1998), hep-ph/9806387.
 - [89] C. S. Lam, *A 2-3 symmetry in neutrino oscillations*, Phys. Lett. **B507**, 214 (2001), hep-ph/0104116.
 - [90] W. Grimus and L. Lavoura, *Maximal atmospheric neutrino mixing and the small ratio of muon to tau mass*, J. Phys. **G30**, 73 (2004), hep-ph/0309050.
 - [91] E. Ma and G. Rajasekaran, *Softly broken $A(4)$ symmetry for nearly degenerate neutrino masses*, Phys. Rev. **D64**, 113012 (2001), hep-ph/0106291.
 - [92] G. Altarelli and F. Feruglio, *Discrete Flavor Symmetries and Models of Neutrino Mixing*, (2010), 1002.0211.
 - [93] K. A. Hochmuth, S. T. Petcov, and W. Rodejohann, $U_{\text{PMNS}} = U_\ell^\dagger U_\nu$, Phys. Lett. **B654**, 177 (2007), 0706.2975.
 - [94] S.-F. Ge, H.-J. He, and F.-R. Yin, *Common Origin of Soft mu-tau and CP Breaking in Neutrino Seesaw and the Origin of Matter*, (2010), 1001.0940.
 - [95] S. Antusch, J. Kersten, M. Lindner, M. Ratz, and M. A. Schmidt, *Running neutrino mass parameters in see-saw scenarios*, JHEP **03**, 024 (2005), hep-ph/0501272.
 - [96] S. F. King, *Tri-bimaximal Neutrino Mixing and θ_{13}* , Phys. Lett. **B675**, 347 (2009), 0903.3199.
 - [97] S. Bertolini, T. Schwetz, and M. Malinsky, *Fermion masses and mixings in $SO(10)$ models and the neutrino challenge to SUSY GUTs*, Phys. Rev. **D73**, 115012 (2006), hep-ph/0605006.
 - [98] C. H. Albright, *Overview of Neutrino Mixing Models and Ways to Differentiate among Them*, (2009), 0905.0146.
 - [99] K. Anderson *et al.*, *White paper report on using nuclear reactors to search for a value of θ_{13}* , (2004), hep-ex/0402041.
 - [100] R. N. Mohapatra *et al.*, *Theory of neutrinos: A white paper*, Rept. Prog. Phys. **70**, 1757 (2007), hep-ph/0510213.
 - [101] G. L. Fogli, E. Lisi, A. Marrone, A. Palazzo, and A. M. Rotunno, *SNO, KamLAND and neutrino oscillations: θ_{13}* , (2009), 0905.3549.
 - [102] T.-K. Kuo and J. T. Pantaleone, *The solar neutrino problem and three neutrino oscillations*, Phys. Rev. Lett. **57**, 1805 (1986).
 - [103] X. Shi and D. N. Schramm, *Solar neutrinos and the MSW effect for three neutrino mixing*, Phys. Lett. **B283**, 305 (1992).

- [104] S. Goswami and A. Y. Smirnov, *Solar neutrinos and 1-3 leptonic mixing*, Phys. Rev. **D72**, 053011 (2005), hep-ph/0411359.
- [105] M. Maltoni, T. Schwetz, M. A. Tortola, and J. W. F. Valle, *Status of global fits to neutrino oscillations*, New J. Phys. **6**, 122 (2004), hep-ph/0405172.
- [106] A. B. Balantekin and D. Yilmaz, *Contrasting solar and reactor neutrinos with a non-zero value of θ_{13}* , J. Phys. **G35**, 075007 (2008), 0804.3345.
- [107] M. Maltoni, T. Schwetz, M. A. Tortola, and J. W. F. Valle, *Status of three-neutrino oscillations after the SNO-salt data*, Phys. Rev. **D68**, 113010 (2003), hep-ph/0309130.
- [108] A. Serenelli, S. Basu, J. W. Ferguson, and M. Asplund, *New Solar Composition: The Problem With Solar Models Revisited*, (2009), 0909.2668.
- [109] Super-Kamiokande, R. Wendell *et al.*, *Atmospheric neutrino oscillation analysis with sub-leading effects in Super-Kamiokande I, II, and III*, (2010), 1002.3471.
- [110] S. T. Petcov, *Diffractive-like (or parametric-resonance-like?) enhancement of the earth (day-night) effect for solar neutrinos crossing the earth core*, Phys. Lett. **B434**, 321 (1998), hep-ph/9805262.
- [111] E. K. Akhmedov, *Parametric resonance of neutrino oscillations and passage of solar and atmospheric neutrinos through the earth*, Nucl. Phys. **B538**, 25 (1999), hep-ph/9805272.
- [112] E. K. Akhmedov, A. Dighe, P. Lipari, and A. Y. Smirnov, *Atmospheric neutrinos at Super-Kamiokande and parametric resonance in neutrino oscillations*, Nucl. Phys. **B542**, 3 (1999), hep-ph/9808270.
- [113] M. Chizhov, M. Maris, and S. T. Petcov, *On the oscillation length resonance in the transitions of solar and atmospheric neutrinos crossing the earth core*, (1998), hep-ph/9810501.
- [114] M. V. Chizhov and S. T. Petcov, *New conditions for a total neutrino conversion in a medium*, Phys. Rev. Lett. **83**, 1096 (1999), hep-ph/9903399.
- [115] M. V. Chizhov and S. T. Petcov, *Enhancing mechanisms of neutrino transitions in a medium of nonperiodic constant-density layers and in the earth*, Phys. Rev. **D63**, 073003 (2001), hep-ph/9903424.
- [116] E. K. Akhmedov, M. Maltoni, and A. Y. Smirnov, *1-3 leptonic mixing and the neutrino oscillograms of the Earth*, JHEP **05**, 077 (2007), hep-ph/0612285.
- [117] C. W. Kim and U. W. Lee, *Comment on the possible electron-neutrino excess in the Super-Kamiokande atmospheric neutrino experiment*, Phys. Lett. **B444**, 204 (1998), hep-ph/9809491.
- [118] O. L. G. Peres and A. Y. Smirnov, *Testing the solar neutrino conversion with atmospheric neutrinos*, Phys. Lett. **B456**, 204 (1999), hep-ph/9902312.
- [119] O. L. G. Peres and A. Y. Smirnov, *Atmospheric neutrinos: LMA oscillations, U_{e3} induced interference and CP-violation*, Nucl. Phys. **B680**, 479 (2004), hep-ph/0309312.
- [120] M. C. Gonzalez-Garcia, M. Maltoni, and A. Y. Smirnov, *Measuring the deviation of the 2-3 lepton mixing from maximal with atmospheric neutrinos*, Phys. Rev. **D70**, 093005 (2004), hep-ph/0408170.
- [121] E. K. Akhmedov, M. Maltoni, and A. Y. Smirnov, *Neutrino oscillograms of the Earth: effects of 1-2 mixing and CP-violation*, JHEP **06**, 072 (2008), 0804.1466.
- [122] G. L. Fogli, E. Lisi, A. Marrone, and A. Palazzo, *Global analysis of three-flavor neutrino masses and mixings*, Prog. Part. Nucl. Phys. **57**, 742 (2006), hep-ph/0506083.
- [123] M. C. Gonzalez-Garcia and M. Maltoni, *Phenomenology with Massive Neutrinos*, Phys. Rept. **460**, 1 (2008), 0704.1800.
- [124] T. Tabarelli de Fatis, *Prospects of measuring $\sin^2 2\theta_{13}$ and the sign of Δm^2 with a massive magnetized detector for atmospheric neutrinos*, Eur. Phys. J. **C24**, 43 (2002), hep-ph/0202232.
- [125] J.-E. Campagne, M. Maltoni, M. Mezzetto, and T. Schwetz, *Physics potential of the CERN-MEMPHYS neutrino oscillation project*, JHEP **04**, 003 (2007), hep-ph/0603172.
- [126] R. Gandhi *et al.*, *Mass Hierarchy Determination via future Atmospheric Neutrino Detectors*, Phys. Rev. **D76**, 073012 (2007), 0707.1723.
- [127] J. Escamilla, D. C. Latimer, and D. J. Ernst, *Atmospheric, long baseline, and reactor neutrino*

- data constraints on θ_{13}* , Phys. Rev. Lett. **103**, 061804 (2009), 0805.2924.
- [128] Super-Kamiokande, J. Hosaka *et al.*, *Three flavor neutrino oscillation analysis of atmospheric neutrinos in Super-Kamiokande*, Phys. Rev. **D74**, 032002 (2006), hep-ex/0604011.
- [129] T. Schwetz, *Global fits to neutrino oscillation data*, Phys. Scripta **T127**, 1 (2006), hep-ph/0606060.
- [130] M. Maltoni and T. Schwetz, *Three-flavour neutrino oscillation update and comments on possible hints for a non-zero θ_{13}* , (2008), 0812.3161.
- [131] K2K, M. H. Ahn *et al.*, *Search for electron neutrino appearance in a 250-km long-baseline experiment*, Phys. Rev. Lett. **93**, 051801 (2004), hep-ex/0402017.
- [132] MINOS, P. Adamson *et al.*, *Search for active neutrino disappearance using neutral-current interactions in the MINOS long-baseline experiment*, Phys. Rev. Lett. **101**, 221804 (2008), 0807.2424.
- [133] P. Huber, M. Lindner, and W. Winter, *Simulation of long-baseline neutrino oscillation experiments with GLOBES*, Comput. Phys. Commun. **167**, 195 (2005), hep-ph/0407333.
- [134] P. Huber, J. Kopp, M. Lindner, M. Rolinec, and W. Winter, *New features in the simulation of neutrino oscillation experiments with GLOBES 3.0*, Comput. Phys. Commun. **177**, 432 (2007), hep-ph/0701187.
- [135] J. A. A. Boehm, *Measurement of electron neutrino appearance with the MINOS experiment*, FERMILAB-THESIS-2009-17.
- [136] R. Acquafredda *et al.*, *The OPERA experiment in the CERN to Gran Sasso neutrino beam*, JINST **4**, P04018 (2009).
- [137] M. Komatsu, P. Migliozi, and F. Terranova, *Sensitivity to $\Theta(13)$ of the CERN to Gran Sasso neutrino beam*, J. Phys. **G29**, 443 (2003), hep-ph/0210043.
- [138] P. Huber, M. Lindner, M. Rolinec, T. Schwetz, and W. Winter, *Prospects of accelerator and reactor neutrino oscillation experiments for the coming ten years*, Phys. Rev. **D70**, 073014 (2004), hep-ph/0403068.
- [139] A. Mereghaglia and A. Rubbia, *Neutrino oscillation physics at an upgraded CNGS with large next generation liquid argon TPC detectors*, JHEP **11**, 032 (2006), hep-ph/0609106.
- [140] B. Baibussinov *et al.*, *A new, very massive modular Liquid Argon Imaging Chamber to detect low energy off-axis neutrinos from the CNGS beam. (Project MODULAR)*, Astropart. Phys. **29**, 174 (2008), 0704.1422.
- [141] R. Battiston, M. Mezzetto, P. Migliozi, and F. Terranova, *European facilities for accelerator neutrino physics: perspectives for the decade to come*, (2009), 0912.3372.
- [142] The MINOS, P. Adamson *et al.*, *New constraints on muon-neutrino to electron-neutrino transitions in MINOS*, (2010), 1006.0996.
- [143] F. Ardellier *et al.*, *Letter of intent for Double-CHOOZ: A search for the mixing angle θ_{13}* , (2004), hep-ex/0405032.
- [144] C. L. Cowan, F. Reines, F. B. Harrison, H. W. Kruse, and A. D. McGuire, *Detection of the free neutrino: A Confirmation*, Science **124**, 103 (1956).
- [145] CHOOZ, M. Apollonio *et al.*, *Initial Results from the CHOOZ Long Baseline Reactor Neutrino Oscillation Experiment*, Phys. Lett. **B420**, 397 (1998), hep-ex/9711002.
- [146] C. Bemporad, G. Gratta, and P. Vogel, *Reactor-based neutrino oscillation experiments*, Rev. Mod. Phys. **74**, 297 (2002), hep-ph/0107277.
- [147] F. X. Hartmann, *Low Level Scintillators and Gadolinium*, Presentation at the Workshop on Future Low Energy Neutrino Experiments, TU Munich, Munich, 9-11 October (2003).
- [148] G. Mention, T. Lasserre, and D. Motta, *A unified analysis of the reactor neutrino program towards the measurement of the θ_{13} mixing angle*, (2007), 0704.0498.
- [149] L. A. Mikaelyan and V. V. Sinev, *Neutrino oscillations at reactors: What next?*, Phys. Atom. Nucl. **63**, 1002 (2000), hep-ex/9908047.
- [150] V. Martemyanov, L. Mikaelyan, V. Sinev, V. Kopeikin, and Y. Kozlov, *The Kr2Det project: Search for mass-3 state contribution $|U(e3)|^2$ to the electron neutrino using a one reactor - two*

- detector oscillation experiment at Krasnoyarsk underground site. ((B)), Phys. Atom. Nucl. **66**, 1934 (2003), hep-ex/0211070.
- [151] H. Minakata, H. Sugiyama, O. Yasuda, K. Inoue, and F. Suekane, *Reactor measurement of θ_{13} and its complementarity to long-baseline experiments*, Phys. Rev. **D68**, 033017 (2003), hep-ph/0211111.
- [152] P. Huber, M. Lindner, T. Schwetz, and W. Winter, *Reactor Neutrino Experiments Compared to Superbeams*, Nucl. Phys. **B665**, 487 (2003), hep-ph/0303232.
- [153] T. Hagner *et al.*, *Muon induced production of radioactive isotopes in scintillation detectors*, Astropart. Phys. **14**, 33 (2000).
- [154] NOMAD, P. Astier *et al.*, *Search for $\nu_{\mu} \rightarrow \nu_e$ oscillations in the NOMAD experiment*, Phys. Lett. **B570**, 19 (2003), hep-ex/0306037.
- [155] NOMAD, J. Altegoer *et al.*, *The NOMAD experiment at the CERN SPS*, Nucl. Instrum. Meth. **A404**, 96 (1998).
- [156] T. Nakadaira, *Status of J-Parc Neutrino Program: T2K*, Presentation at Les Rencontres de Physique de la Valle d'Aoste, La Thuile, 28 February–6 March (2010).
- [157] A. K. Mann *et al.*, *Long baseline neutrino oscillation experiment at the AGS: Proposal*, BNL-PROPOSAL-889.
- [158] P. Huber, M. Mezzetto, and T. Schwetz, *On the impact of systematical uncertainties for the CP violation measurement in superbeam experiments*, JHEP **03**, 021 (2008), 0711.2950.
- [159] Minerva, D. Drakoulakos *et al.*, *Proposal to perform a high-statistics neutrino scattering experiment using a fine-grained detector in the NuMI beam*, (2004), hep-ex/0405002.
- [160] M. Messier, private communication, March 2010.
- [161] T. Sekiguchi, *Neutrino beamline for T2K*, AIP Conf. Proc. **981**, 275 (2008).
- [162] NA61, M. Posiadala, *Status of the NA61 (SHINE) experiment at CERN*, (2009), 0901.3332.
- [163] HARP, M. G. Catanesi *et al.*, *The HARP detector at the CERN PS*, Nucl. Instrum. Meth. **A571**, 527 (2007).
- [164] HARP, M. G. Catanesi *et al.*, *Measurement of the production cross-section of positive pions in p Al collisions at 12.9-GeV/c*, Nucl. Phys. **B732**, 1 (2006), hep-ex/0510039.
- [165] M. G. Catanesi *et al.*, *Measurement of the production cross-section of positive pions in the collision of 8.9 GeV/c protons on beryllium*, Eur. Phys. J. **C52**, 29 (2007), hep-ex/0702024.
- [166] NOvA, web-page: <http://www-nova.fnal.gov>.
- [167] P. Huber, M. Lindner, T. Schwetz, and W. Winter, *First hint for CP violation in neutrino oscillations from upcoming superbeam and reactor experiments*, JHEP **11**, 044 (2009), 0907.1896.
- [168] P. Huber, M. Lindner, and W. Winter, *Synergies between the first-generation JHF-SK and NuMI superbeam experiments*, Nucl. Phys. **B654**, 3 (2003), hep-ph/0211300.
- [169] H. Minakata, H. Nunokawa, and S. J. Parke, *The complementarity of eastern and western hemisphere long-baseline neutrino oscillation experiments*, Phys. Rev. **D68**, 013010 (2003), hep-ph/0301210.
- [170] O. Mena, H. Nunokawa, and S. J. Parke, *NOvA and T2K: The race for the neutrino mass hierarchy*, Phys. Rev. **D75**, 033002 (2007), hep-ph/0609011.
- [171] A. Cervera *et al.*, *Golden measurements at a neutrino factory*, Nucl. Phys. **B579**, 17 (2000), hep-ph/0002108.
- [172] M. Freund, *Analytic approximations for three neutrino oscillation parameters and probabilities in matter*, Phys. Rev. **D64**, 053003 (2001), hep-ph/0103300.
- [173] E. K. Akhmedov, R. Johansson, M. Lindner, T. Ohlsson, and T. Schwetz, *Series expansions for three-flavor neutrino oscillation probabilities in matter*, JHEP **04**, 078 (2004), hep-ph/0402175.
- [174] T. Kajita, H. Minakata, and H. Nunokawa, *Method for determination of $|U_{e3}|$ in neutrino oscillation appearance experiments*, Phys. Lett. **B528**, 245 (2002), hep-ph/0112345.
- [175] K. B. M. Mahn and M. H. Shaevitz, *Comparisons and combinations of reactor and long-baseline neutrino oscillation measurements*, Int. J. Mod. Phys. **A21**, 3825 (2006), hep-ex/0409028.

- [176] P. Huber and T. Schwetz, *Precision spectroscopy with reactor anti-neutrinos*, Phys. Rev. **D70**, 053011 (2004), hep-ph/0407026.
- [177] M. Mezzetto, *Next Challenge in Neutrino Physics: the θ_{13} Angle*, (2009), 0905.2842.
- [178] A. Suzuki, *KamLAND and T2K*, Prog. Part. Nucl. Phys., In Press, Corrected Proof (2010).
- [179] T. Schwetz and W. Winter, *Testing mass-varying neutrinos with reactor experiments*, Phys. Lett. **B633**, 557 (2006), hep-ph/0511177.
- [180] J. Kopp, M. Lindner, T. Ota, and J. Sato, *Non-standard neutrino interactions in reactor and superbeam experiments*, Phys. Rev. **D77**, 013007 (2008), 0708.0152.
- [181] T. Schwetz, *What is the probability that θ_{13} and CP violation will be discovered in future neutrino oscillation experiments?*, Phys. Lett. **B648**, 54 (2007), hep-ph/0612223.
- [182] M. Ishitsuka, T. Kajita, H. Minakata, and H. Nunokawa, *Resolving Neutrino Mass Hierarchy and CP Degeneracy by Two Identical Detectors with Different Baselines*, Phys. Rev. **D72**, 033003 (2005), hep-ph/0504026.
- [183] A. Badertscher *et al.*, *A Possible Future Long Baseline Neutrino and Nucleon Decay Experiment with a 100 kton Liquid Argon TPC at Okinoshima using the J-PARC Neutrino Facility*, 2008.
- [184] M. Diwan *et al.*, *Proposal for an experimental program in neutrino physics and proton decay in the homestake laboratory*, 2006.
- [185] O. Bruning *et al.*, *Lhc luminosity and energy upgrade: A feasibility study.*, CERN-LHC-PROJECT-REPORT-626;.
- [186] M. Meddahi and E. Shaposhnikova, *Analysis of the maximum potential proton flux to cngs*, CERN-AB-2007-013, 2007.
- [187] J. J. Gomez-Cadenas *et al.*, *Physics potential of very intense conventional neutrino beams*, 2001.
- [188] B. Autin *et al.*, *Conceptual design of the SPL, a high-power superconducting H- linac at CERN*, CERN-2000-012.
- [189] A. de Bellefon *et al.*, *MEMPHYS: A large scale water Cerenkov detector at Frejus*, 2006.
- [190] A. Rubbia, *A CERN-based high-intensity high-energy proton source for long baseline neutrino oscillation experiments with next- generation large underground detectors for proton decay searches and neutrino physics and astrophysics*, 2010.
- [191] *Large apparatus studying grand unification and neutrino astrophysics*, <http://www.laguna-science.eu/>.
- [192] V. Barger, P. Huber, D. Marfatia, and W. Winter, *Which long-baseline neutrino experiments are preferable?*, Phys. Rev. **D76**, 053005 (2007), hep-ph/0703029.
- [193] S. Choubey, P. Coloma, A. Donini, and E. Fernandez-Martinez, *Optimized Two-Baseline Beta-Beam Experiment*, JHEP **12**, 020 (2009), 0907.2379.
- [194] A. D. Bross, M. Ellis, S. Geer, O. Mena, and S. Pascoli, *A Neutrino factory for both large and small θ_{13}* , Phys. Rev. **D77**, 093012 (2008), 0709.3889.
- [195] M. Mezzetto, *Physics potential of the gamma = 100,100 beta beam*, Nucl. Phys. Proc. Suppl. **155**, 214 (2006), hep-ex/0511005.
- [196] M. Mezzetto, *SPL and beta beams to the Frejus*, Nucl. Phys. Proc. Suppl. **149**, 179 (2005).
- [197] J. Burguet-Castell, D. Casper, J. J. Gomez-Cadenas, P. Hernandez, and F. Sanchez, *Neutrino oscillation physics with a higher gamma beta- beam*, Nucl. Phys. **B695**, 217 (2004), hep-ph/0312068.
- [198] J. Burguet-Castell, D. Casper, E. Couce, J. J. Gomez-Cadenas, and P. Hernandez, *Optimal beta-beam at the CERN-SPS*, Nucl. Phys. **B725**, 306 (2005), hep-ph/0503021.
- [199] S. Geer, *Muon Colliders and Neutrino Factories*, Ann. Rev. Nucl. Part. Sci. **59**, 347 (2009).
- [200] A. Cervera, F. Dydak, and J. Gomez Cadenas, *A large magnetic detector for the neutrino factory*, Nucl. Instrum. Meth. **A451**, 123 (2000).
- [201] A. Cervera, A. Laing, J. Martin-Albo, and F. J. P. Soler, *Performance of the MIND detector at a Neutrino Factory using realistic muon reconstruction*, 2010.
- [202] A. De Rujula, M. B. Gavela, and P. Hernandez, *Neutrino oscillation physics with a neutrino factory*, Nucl. Phys. **B547**, 21 (1999), hep-ph/9811390.